

Optimization of Tapered Deployable Space Structures

Srivatsa Harish

Thesis submitted to the faculty of the Virginia Polytechnic Institute and State University in
partial fulfillment of the requirements of the degree of

Master of Science

In

Aerospace Engineering

Rakesh K. Kapania, Chair

H. Pat Artis

Daisaku Inoyama

May 7, 2025

Blacksburg, Virginia

Keywords: Deployable Structure, Optimization, Finite Element Analysis, Space Structure

Optimization of Tapered Deployable Space Structures

Srivatsa Harish

ABSTRACT

Modern spacecraft utilize deployable structures for many applications to strike a balance between functionality and size within a launch vehicle. Due to volume restrictions in a launch vehicle these deployable structures are stowed in a collapsed configuration during launch and deployed when the spacecraft successfully reaches a stable orbit. In this study, an optimization of a tapered composite beam deployable structure is performed to find an optimally performing design, minimizing wrapped strain energy and deployment dynamics. The beam will consist of a compressible, lenticular section that will include a taper ratio from the beam's root to its tip in a chord-wise manner. Material selection of the composite layup will also be included in the optimization with the ability to choose different composite mixtures, layup directions and ply thicknesses. Abaqus CAE, a commercial finite element analysis software, is used to conduct two analyses that make up the optimization architecture. The first analysis is to obtain the fundamental frequency of a beam design in its deployed state. The second will find stresses along the beam as it is wrapped examining the stored strain energy of the beam in the wrapped state. The second analysis will then continue to deploy the structure from its wrapped state and examine the rotational velocity and beam's oscillatory behavior during deployment. HEEDS MDO, a commercial optimization software, is utilized to conduct the optimization. Design variables will include beam dimensions and taper ratio, as well as material properties of the composite layup. The objective function will minimize the beam's weight, stored strained energy in the wrapped state and beam tip displacements during deployment. Constraints will be assigned on design variables, deployed system rotational velocity and transient stresses during wrapping will be checked for material failure using Hashin Damage Criterion. Finding a design that satisfies mission requirements and maintains structural integrity during wrapping and deployment will be challenging and computationally expensive. The optimization simulation presented in this paper aims to generate the best possible design that satisfies all requirements.

Optimization of Tapered Deployable Space Structures

Srivatsa Harish

GENERAL AUDIENCE ABSTRACT

Launch vehicles are used to launch a variety of spacecraft into orbit. Certain components of the spacecraft like solar arrays, booms and antennas must be large to perform their functional duties on orbit, but they must also be stored such that they fit in the launch vehicle volume. A common way to reduce volume of these components is to use a deployable structure to reduce the footprint of the component for launch and then deploy these structures once a stable orbit has been achieved. The objective of this research effort is to develop a streamlined optimization approach to digitally trade designs for such deployable structures to meet mission requirements and maintain structural integrity. The analysis efforts in the optimization consists of a modal analysis to determine deployed fundamental mode of the system and a dynamic analysis that determines structural characteristics of the beam when it is wrapped for stowage and subsequently deployed. The optimization is conducted using HEEDS MDO, a commercially available optimization tool. The individual analyses are done using ABAQUS CAE, a commercially available Finite Element Method software. The system analyzed will consist of a rectangular spacecraft bus attached to a central cylindrical hub that the deployable structure will wrap around. The deployable structure consists of a flexible, lenticular composite beam that will include a root-to-tip taper in in the chordwise direction. This taper will allow the beam to have a linear taper from root-to-tip, with the optimization able to assess different levels of taper aggressiveness. Other parameters of the beam will also be assessed, including the lenticular cross-sectional parameters and material properties of the composite beam. Constraints will be placed on the fundamental mode of the deployed beam system to ensure the system remains stiff enough to stratify general mission requirements. The beam's stored strain energy and Hashin Damage initiation will also be monitored as the beam is wrapped around the hub. The tracked Hashin Damage initiation ensures that the chosen composite material property strength is not being exceeded while the beam is wrapped. After the beam is allowed to deploy, the number of beam tip oscillations will be counted, as well as the overall system rotational velocity. Using these outputs, the optimization will aim to minimize the strain energy stored in the beam, the beam's overall weight, and the number to beam oscillations after deployment. A beam that meets these objectives and adheres to the constraints will be the final product of the optimization.

Dedication

This paper is dedicated to my parents, Harish and Shubha Baipadithaya, who helped me keep a level head while balancing my research efforts, academic course work and obligations at work. They taught me that hard work is required for things that are valuable and to reward the friction in effort, rather than just the result. I thank them for their patience and kind support during the writing of this thesis.

Acknowledgments

I would like to thank Dr. Rakesh Kapania of Virginia Polytechnic Institute and State University for his guidance on this research effort. He has afforded me the opportunity to study and learn the intricacies of structural mechanics under him, providing me valuable feedback when I needed it and allowing me to explore concepts on my own.

I would also like to thank my managers Dr. Daisaku Inoyama and Dr. Tom Stoumbos of Northrop Grumman Corporation for their strong support and encouraging me to pursue this degree. Without them, this paper may not have existed. I thank them for providing me their valuable guidance in keeping my work in scope and showing me how parts of my research can be applied in practical engineering. I have learned a great deal from them both, and this paper is a reflection of that.

Table of Contents

Dedication.....	iv
Acknowledgments.....	v
Table of Contents.....	vi
List of Figures.....	viii
List of Tables.....	xi
I. Introduction.....	1
A. Background and Motivation.....	1
B. Optimization Problem Formulation.....	4
II. Literature Review.....	6
III. Methods of Analysis.....	10
A. Abaqus CAE Modeling & Setup.....	10
B. Layup Material Property Selection.....	14
C. Optimization.....	15
IV. Results & Discussion.....	18
A. Preliminary Optimization Study.....	18
B. Optimization Results.....	21
1. Best Feasible Beam Design.....	21
2. Objective Function Parameter Correlation.....	23

3.	Input/Output Parameter Correlation	25
4.	Influence Charts	40
5.	Producibility of Feasible Designs	47
C.	Local vs Global Optimum.....	48
V.	Conclusion & Future Work	50
VI.	Bibliography	54
	Appendix A: Hashin Damage Initiation Criteria	58
	Appendix B: HEEDS Material Property Selection Repository	59
	Appendix C: Preliminary Optimization Figures	60
	Appendix D: Additional Sobol Index Plots	66

List of Figures

Figure 1: Model set-up and dimensions of rib and hub (a) & (b), cross-section of lenticular beam root (c) and chordwise taper ratio application (d).....	4
Figure 2: Assembly of wrapping and deployment Abaqus CAE model.....	11
Figure 3: Abaqus CAE Explicit Dynamics model at wrapped state (a) and during deployment (b)	12
Figure 4: Constraint and load application points for wrapping and deployment model.....	13
Figure 5: The initial shape for the frequency model (a) and the deformed first mode of frequency (b).....	14
Figure 6: Flowchart of HEEDS Optimization architecture.....	16
Figure 7: Preliminary optimization algorithm flowchart.....	19
Figure 8: Preliminary Study Best Feasible Root cross-section.....	20
Figure 9: Best Feasible design from the Main Optimization.....	22
Figure 10: Objective Function Correlations for Weight vs Strain Energy (a), Strain Energy vs Beam Tip Displacements (b), Weight vs Beam Tip Displacements (c).	24
Figure 11: Parameter Correlation for Taper Ratio vs Weight (a), Strain Energy (b), Frequency (c), Rotation Rate (d), Tip Displacements (e).	26
Figure 12: Parameter Correlation for Ply Thickness vs Weight (a), Strain Energy (b), Frequency (c), Rotation Rate (d), Tip Displacements (e).....	28
Figure 13: Parameter Correlation Root θ vs Weight (a), Strain Energy (b), Frequency (c), Rotation Rate (d), Tip Displacements (e).....	30
Figure 14: Parameter Correlation of Outside Fiber Orientation vs Weight (a), Strain Energy (b), Frequency (c), Rotation Rate (d), Tip Displacements (e).....	32

Figure 15: Parameter Correlation of Inside Fiber Orientation vs Weight (a), Strain Energy (b), Frequency (c), Rotation Rate (d), Tip Displacements (e)..... 33

Figure 16: Parameter Correlation of Matrix Selection vs Weight (a), Strain Energy (b), Frequency (c), Rotation Rate (d), Tip Displacements (e)..... 35

Figure 17: Parameter Correlation of Fiber Selection vs Weight (a), Strain Energy (b), Frequency (c), Rotation Rate (d), Tip Displacements (e)..... 36

Figure 18:Parameter Correlation of Boundary Stiffness vs Weight (a), Strain Energy (b), Frequency (c), Rotation Rate (d), Tip Displacements (e)..... 38

Figure 19:Parameter Correlation of Boundary Damping vs Weight (a), Strain Energy (b), Frequency (c), Rotation Rate (d), Tip Displacements (e)..... 39

Figure 20: Boruta Influence Chart for Beam Weight (a) and Fundamental Frequency (b)..... 42

Figure 21: Boruta Influence Chart for Beam Stored Strain Energy..... 43

Figure 22: Boruta Influence Chart for Beam Weight (a) and Fundamental Frequency (b)..... 44

Figure 23: Sobol Index Chart for Beam Tip Displacements (a) and Avg Body Rotation (b). 47

Figure 24: Parameter Correlation: Inside Fiber Orientation vs Weight (a), Strain Energy (b) & Frequency (c) 60

Figure 25: Parameter Correlation: Inside Fiber Orientation vs Weight (a), Strain Energy (b) & Frequency (c) 60

Figure 26: Parameter Correlation: Ply Thickness vs Weight (a), Strain Energy (b) & Frequency (c) 62

Figure 27: Parameter Correlation: Root θ vs Weight (a), Strain Energy (b) & Frequency (c).... 62

Figure 28: Parameter Correlation: Taper Ratio vs Weight (a), Strain Energy (b) & Frequency (c) 63

Figure 29: Objective Correlation: Strain Energy vs Weight (a), Frequency vs Strain Energy (b) & Weight vs Frequency (c)..... 64

Figure 30: Parameter Correlation: Fiber Selection vs Weight (a), Strain Energy (b) & Frequency (c) 65

Figure 31: Parameter Correlation: Matrix Selection vs Weight (a), Strain Energy (b) & Frequency (c) 65

Figure 32: Sobol Index Plot Correlation: Beam Weight (a), Strain Energy (b) & Deployed Frequency (c) 67

List of Tables

Table 1: Boundary conditions and loads for wrapping and deployment model	13
Table 2: Material properties chart [19]	15
Table 3: Optimization Parameter range and resolution	17
Table 4: Feasible Composite Ply Thickness & Corresponding Poisson’s ratio [15].....	18
Table 5: Preliminary Optimization Best Feasible design parameters.....	20
Table 6: Main Optimization Best Feasible Design Parameters	22
Table 7: Input Parameter Differences in Main and Auxiliary Optimization Studies	48
Table 8: Parameter Differences in Main and Auxiliary Optimization Studies for Best Feasible Design	49

Nomenclature

f	= generic function
θ	= angle defining the lenticular cross-section
R_1	= radius defining the lenticular cross-section
R_2	= radius defining the lenticular cross-section
t	= thickness of lamina in composite layup
L	= length of lenticular beam
n	= number of plies
h	= height
w	= weight
c_f	= filler volume ratio
$\phi_{1,2}$	= orientation angle of lamina (inside/outside)
ρ	= density
E	= Young's modulus
G	= shear modulus
ν	= Poisson's ratio
s	= root-tip taper ratio (chord-wise)
k	= connector Stiffness
d	= connector Damping
<i>Fiber</i>	= fiber index
<i>Matrix</i>	= matrix index

I. Introduction

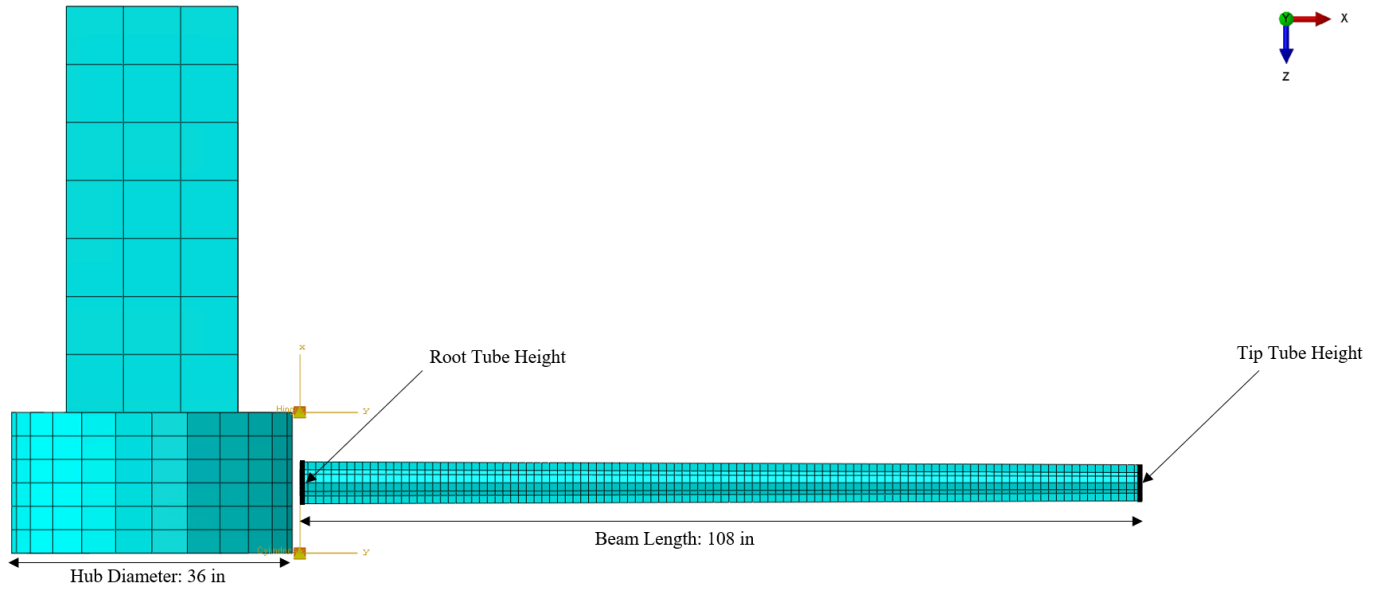
A. Background and Motivation

A careful balance between functionality and size is required to launch spacecraft into orbit. To achieve this balance, modern spacecraft utilize structures known as “deployable structures”. These structures are commonly found as antennas, booms or reflectors that are stowed in a collapsed configuration for launch and are deployed when the spacecraft successfully reaches a stable orbit. Expansion is usually performed by either a mechanical deployment utilizing a truss-rod system or can be deployed using the stored strain energy of the compacted system. Mechanically deployed structures can be expensive, often requiring additional hardware that leads to increased weight and volume in the launch vehicle. Astro Aerospace, a Northrop Grumman subsidiary, has dedicated product lines for large, deployable reflector antennas that use these mechanical deployment mechanisms [1]. Strain energy deployable structures offer the benefit of being less complex, cost less and have lower volume. The expansion from collapsed state to the fully deployed state is a highly dynamic event that employs the use of stored strain energy to unfurl the structure. Smaller satellites benefit from these types of deployables due to the need to reduce weight and volume of the overall spacecraft.

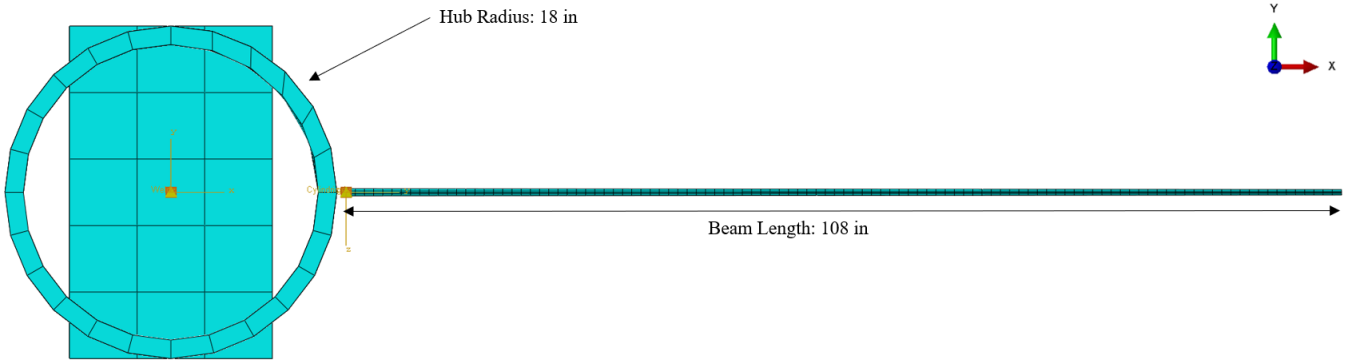
The work presented in this paper is a part of the continued development of an optimization algorithm that aims to deliver an automated design process that focuses on virtual prototyping of complex deployable structures. In previous years, the focus of the optimization algorithm has been on adding the ability to manipulate the lenticular geometry of the beam [2] and the ability to manipulate the material properties of the beam [3]. Both iterations of the effort have had a similar set up in the optimization algorithm that includes running a normal modes analysis and explicit

dynamics analysis consisting of wrapping the composite beam around a central hub. Once the optimization results are derived, the beam design is run in an additional explicit dynamic analysis to analyze deployment of best beam design. The latest attempt discussed in this paper adds functionality to the prior attempts by adding a chordwise tapered cross-section to the lenticular beam and modifying the optimization algorithm to include the deployment analysis within the optimization loop. The end result is to provide an algorithm that can determine the best beam design that will fulfill specified requirements for acoustics, wrapping and deployment of the composite beam.

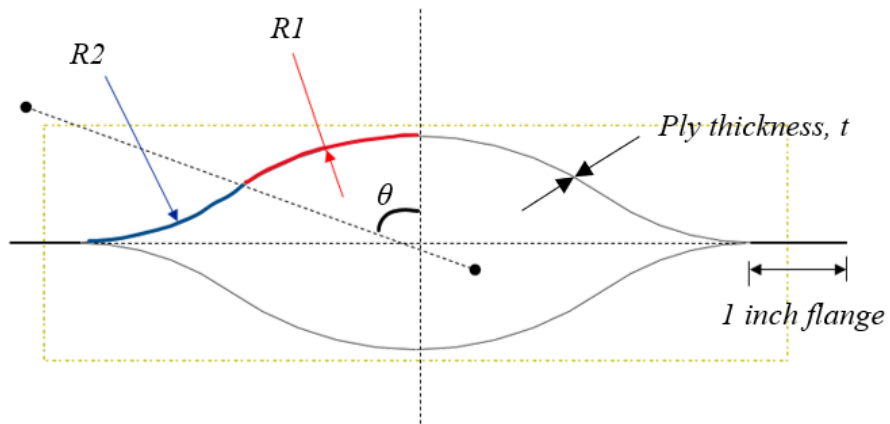
This paper will focus on a structure consisting of a radially mounted lenticular beam that wraps around a central hub prior to being unfurled. The primary shape of the lenticular tubes consists of a tulip-like cross-section that allows for the tube to be compressed and flattened as it is wrapped around the center hub, defined in Figure 1. This is done to reduce the stiffness of the beam for the sake of wrapping but remain stiff enough to complete the intended mission. The strain energy produced by flattening and wrapping the beam with this shape also serves as the energy used to deploy the beam, reducing the hardware required for deployment. Previous iterations of the optimization included a uniform tube cross-section along the length of the beam, but this optimization will include a root-to-tip cross-section taper in the chordwise direction. The tip cross-section parameters will be modified to be scaled down from the root cross-section parameters. To find the best design, a dynamic analysis is performed using the explicit dynamic solver in Abaqus CAE and the optimization is done in HEEDS Multi-disciplinary Optimization (MDO).



(a)



(b)



(c)

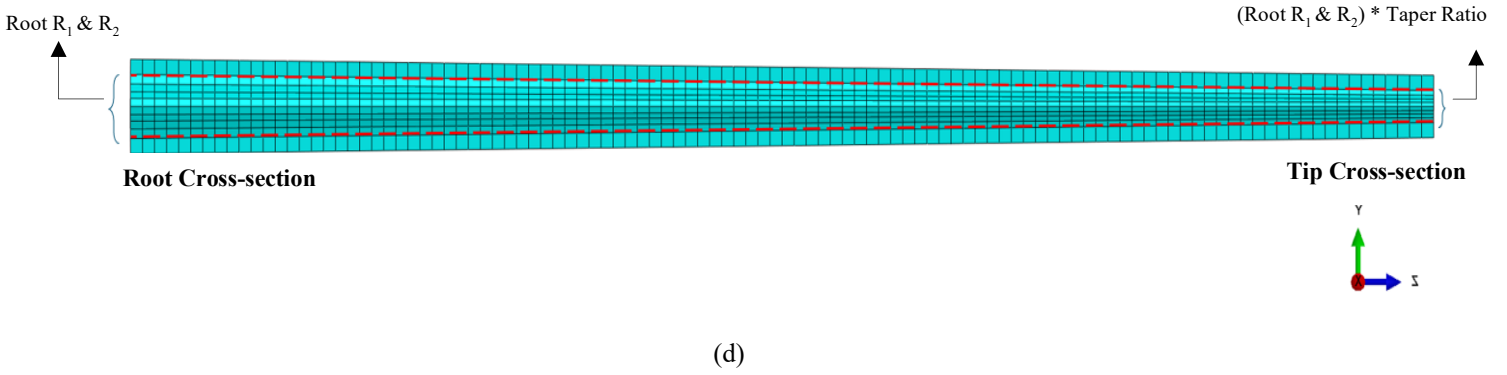


Figure 1: Model set-up and dimensions of rib and hub (a) & (b), cross-section of lenticular beam root (c) and chordwise taper ratio application (d)

The flattened tube with included chordwise taper can be idealized as a trapezoid. Tube root height and tube weight will be calculated algebraically using Equation (1) & (2), utilizing the three parameters that fully constrain tube cross-section (R_1 , R_2 , θ) defined in Figure 1 (c). Height and weight of the tube provide the ability to minimize the weight and constrain the size of the tube.

$$h = [2 * (R_1\theta + R_2\theta) + 2]_{root} + [2 * (R_1\theta + R_2\theta) + 2]_{tip} \quad (1)$$

$$w = \frac{h}{2} * L * t * n * \rho_{eff} * g \quad (2)$$

A linear, chordwise taper is applied to the beam by applying a taper ratio to the tip cross-section based on root cross-section R_1 and R_2 parameters. The taper ratio is defined as a percentage of the root R_1 and R_2 parameters i.e., 20% to 100% of those values. Figure 1 (d) aims to show how this taper ratio is applied to the tip R_1 and R_2 parameters. The θ quantity does not have a scale factor applied to keep the beam's taper uniform.

B. Optimization Problem Formulation

The objective function designed for this paper is shown in Equation 1.1. Reconfiguring the objective function was necessary as compared to previous research, where deployment characteristics of the wrapped beam were not part of the optimization [1,3,4]. In this study, the

goal will be to minimize weight of the beam, strain energy, and the tip displacement peaks during deployment. Design parameters from both the geometry and material selection are used in the objective function formulation and are subjected to the constraints shown.

Minimize:

$$\frac{f_1(R_1, R_2, \theta, t, s, c_f, Matrix, Fiber, \rho_{eff})}{f_{1_0}} + \frac{f_2(R_1, R_2, \theta, t, Matrix, Fiber, c_f, \phi_1, \phi_2, s)}{f_{2_0}} + \frac{f_3(R_1, R_2, \theta, t, Matrix, Fiber, c_f, \phi_1, \phi_2, s, k, d)}{f_{3_0}} \quad (1.1)$$

Where,

$$f_{n_0} = \text{Initial value of } f_n \quad (1.2)$$

$$f_1 = \text{Tube weight} \quad (1.3)$$

$$f_2 = \text{Stored strain energy} \quad (1.4)$$

$$f_3 = \text{Tip displacement peaks} \quad (1.5)$$

Subject To:

$$\text{Tube weight} < 3 \text{ lb} \quad (1.6)$$

$$\text{First Mode Frequency} > 0.5 \text{ Hz} \quad (1.7)$$

$$\text{Average spacecraft body rotation} < 3^\circ/\text{s} \quad (1.8)$$

$$\text{Hashin Fiber Compression} < 0.7 \quad (1.9)$$

$$\text{Hashin Fiber Tension} < 0.7 \quad (1.10)$$

$$\text{Hashin Matrix Tension} < 0.7 \quad (1.11)$$

$$\text{Hashin Matrix Compression} < 0.7 \quad (1.12)$$

The constraints of the optimization are set based on the satisfaction of the survival of the beam design during wrapping and deployment, as well as general mission requirements for a deployable

space structure. The mission requirement is satisfied by setting a minimum for the fundamental mode of the deployed structure. Space structures with fundamental mode below 0.5 Hz can be considered low frequency and undesirable due to their ability to be easily excited and cause potential dynamic coupling on orbit. The mission requirement is also satisfied by preventing excess rotation of the spacecraft due to deployment of the space structure. The spacecraft analyzed in this optimization is roughly 500kg and typical Reaction Wheel Assemblies (RWAs) designed for spacecraft of this mass range have an angular momentum capacity of ~ 4 N-m-s [5]. Thus, the spacecraft must not exceed an average body rotation of 3 °/s to recover from a tumble rate using only RWAs. The optimization will constrain the deployment dynamics of the system such that a feasible design will have an average body rotation less than 3 °/s.

Survival of the structure as it is wrapped is ensured by looking at the Hashin composite damage initiation criterion that is observed as an output from Abaqus CAE. Hashin Damage initiation criteria definitions can be referenced in Appendix A, per the Abaqus CAE manual. This output is processed via a Python script that recovers the maximum value for fiber tension, fiber compression, matrix tension, matrix compression during wrapping. Material failure will occur if the maximum damage criteria is greater than or equal to 1.0. For this optimization, a value of 0.7 is used as the constraint to include a factor of safety of 1.43 to the beam design. The optimization will run a select number of iterations and find the best feasible design that satisfies these constraints and objectives.

II. Literature Review

Space deployables have been in development since the early 1980s, designed to be flexible or rigid depending on the application on orbit [6]. Rigid deployables use mechanisms in conjunction with linkages and hinges to actively deploy the structure on orbit. Flexible deployables, like the one

investigated in this paper, rely on the stored potential energy from a method of stowing to passively deploy the structure without the use of complex mechanisms. With advancements in manufacturing, a combination of flexible materials and rigid components allow for semi-rigid deployables with inbuilt actuators to aid in the deployment of complex truss structures [7]. However, the cost of such rigid structures can be the complexity of adding mechanical components, potentially increasing the number of failure points during deployment. Another cost is the additional hardware weight associated with deployables with actuators and mechanisms to manage deployment. Flexible deployable structures without deployment mechanisms are less complex and save weight due to the lack of additional hardware required. Understanding of the viscoelastic behavior of thin-ply, high strain composites, like the one presented in this paper, is important to accurately predict and understand the strain energy stored in the beam as it is stowed. Francis, W H et al. [8] provides insight on this behavior with qualification testing of thin-ply composite structures. Using testing fixtures to bend the composite material, they were able to establish instant failure curvature limits and better understand stress-relaxation effects. They also conducted experiences on Diametric Compression Testing (DCT) to better understand the strain energy and creep effects in a composite tube, which were successfully correlated to analysis.

An example of a flexible deployable structure reliant on the stored energy during the stowing process is one investigated by Winter et. al. [9]. This study investigated rolling strategies to stow a flexible solar array called PowerSail to reduce the complexity and weight of creating a deployable with mechanical components to aid in deployment. The deployment was facilitated by shape memory longerons that were sequentially heated to unroll the solar array at a controlled rate and lock the unraveled structure into place with high stiffness members. A similar approach is used in the continued effort in developing the Habitable Exoplanet Observatory (HabEx) starshade at

NASA JPL. The proposal for the starshade includes an array of petal-like structures that wrap around a central hub, similar to the setup of the deployable system presented in this paper [10]. The design consists of a center disk that all petals attach to at the core of the structure. The deployment starts by first expanding the petals and then continues to spin the central disk to fully deploy the rest of the starshade with the aid of center truss system. This shows an example of a deployable structure that combines flexibility at some parts and utilizes mechanisms to aid its full deployment. Another deployable structure design is the Mars Express Sub-Surface Sounding Radar Altimeter (MARSIS) boom. The study conducted by Mobrem and Adams [11] details the design and performance of a two 20-meter deployable booms. Each boom was used for mapping of the Martian sub-surface structure. The design of the boom has a similar lenticular opening discussed in this paper, leveraging strain energy in the structure to drive deployment. The deployment of flexible structures is not without issues, however. Due to the nonlinear nature of the deployment, unexpected behavior can be seen during orbital deployment. This unexpected behavior was seen in the MARSIS dual lenticular boom deployment. The on orbit deployment showed the expected angular rate of the spacecraft from simulation for the first 2 seconds but quickly deviated from the simulation results in the final six seconds of deployment. Though the appropriate assumptions were made for the damping included in the simulation of the boom's deployment, the flight data showed the constant angular rate in simulation was held for roughly 4 seconds less than simulation suggested. The PowerSail, HabEx starshade and MARSIS boom all serve as inspiration for model set up studied in this paper. The on-orbit deployment observations from the MARSIS also highlights the importance of including the deployment simulation in fully assessing a space deployable structure.

In the method presented in this paper, the optimization software has the ability to choose material properties from a pre-determined set of material combinations, utilizing the work from previous research on this effort [3]. This set of properties is derived from Autodesk Heliuss to compute Young's modulus, Poisson's ratio, density and shear modulus. These parameters are then used to find the effective material properties based on the rule of mixtures. Heliuss' micromechanics calculations are used to assess material strength capabilities of the combination of material properties [12]. Hashin damage initiation criteria are used to contextualize the performance of a particular beam design's ability to wrap in this paper. Hashin damage initiation is described as the onset of degradation at a material point for a fiber reinforced material using the different damage initiation mechanisms from effective stress tensor. This output is easily recovered in ABAQUS CAE [13, 14]. The range of thin-ply composite thickness is found from the research conducted by Neigh in which he describes the range of reference laminates using classifications for thin, intermediate and thick composites [15]. These values are taken to set the range of ply thicknesses in the optimization described in this paper and can be used to describe producibility of a feasible composite beam design from the optimization.

Limited material exists on the optimization of deployable structures. One example is the research conducted by Kwak et. al. that includes optimization of a deployable antenna reflector with the aim to minimize weight of the structure. The optimization was conducted for a single reflector panel and included analysis of the reflector design's performance in stowed and deployed states for particular loading conditions [16]. This was done iteratively, with no mention of the specific optimization search algorithm used. Another work by Fernandes et. al. considers the optimization of an elastic hinge, like ones used in the MARSIS boom [17]. This optimization considered both a modal analysis and a structural model to consider performance of the deployed beam's natural

frequency and its ability to fold at the elastic hinge. The optimization algorithm used a Genetic Algorithm (GA) and Particle Swarm Optimization method (PSO) to conduct global and local search of the design space. This optimization philosophy is similar to the one used in this paper. The work presented in this paper utilizes Siemens SHERPA optimization algorithm. SHERPA algorithm is a hybrid adaptive algorithm that prioritizes efficiency and robustness with the intent to learn the design space by using local and global search methods simultaneously. This allows SHERPA to find optimal solutions with fewer evaluations compared to other algorithms [18]. For this reason, the SHERPA algorithm is chosen as the search algorithm for the optimization described in this paper.

III. Methods of Analysis

A. Abaqus CAE Modeling & Setup

There are a total of two simulations that utilize Abaqus CAE. The first is the wrapping and deployment model, consisting of two individual simulation steps to analyze wrapping of the beam around a cylindrical hub, as well deployment of the beam with the assembly released with 6 degrees of freedom free. During the wrapping step, the transient Hashin damage initiation criteria is calculated, as well as strain energy density of the beam in the wrapped state. The second step, deployment, will observe tip displacement peaks and transient rotational dynamics of the assembly as the beam is released from the wrapped state in six degrees of freedom. Abaqus CAE explicit dynamics solver is used to analyze the nonlinear dynamics in the wrapping and deployment simulation [14]. The second analysis is a standard finite element analysis model that aims to solve the fundamental frequency of the deployed structure consisting of 4 equally spaced beams. The natural frequency and wrapping/deployment simulation are incorporated into HEEDS Multi-

disciplinary Optimization (MDO). HEEDS uses a proprietary SHERPA optimization algorithm to iteratively find the optima given a target number of design iterations to evaluate.

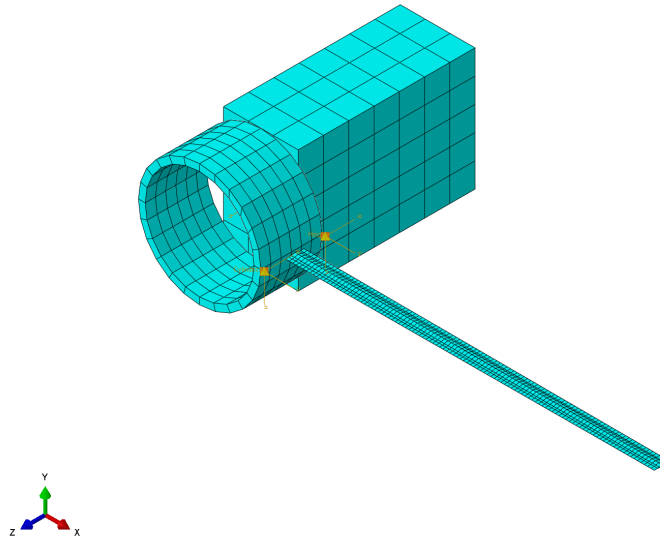


Figure 2: Assembly of wrapping and deployment Abaqus CAE model

The explicit dynamic model includes a lenticular beam, hub and spacecraft bus assembly as depicted in Figure 2. The hub is fixed with a welded joint to a 22 in x 36 in x 52 in cuboid that represents a generic shape of a spacecraft bus. This bus structure and central hub are both modeled as rigid bodies. The terminology “top” and “bottom” will reference features in the positive (top) and negative (bottom) z-directions, respectively. The tube is attached to the protruding edges of the central hub using a hinge connector on the bottom edge and a cylindrical connector on the top. The hinge connector constrains all degrees of freedom except rotation about the z-axis, local to the connection point. The cylindrical connector will do the same but allow for z-axis translation at the connection point as well. This is to allow for expansion of the beam as it is wrapped and gets flattened around the hub. Each connector also has a stop that prevents rotation above the neutral, 0-degree position of the beam. The stop is to prevent re-contact of the beam as it is deployed, restricting the rotation in the radial direction. The connectors also have stiffness and damping

values that are treated as design variables in the optimization. The stops and the connector stiffness/damping both aim to reduce the settling time for the beam as it is unfurled and reduce the rotation induced by the deployment. Figure 3 shows the wrapping and deployment step that compose the explicit dynamics simulation.

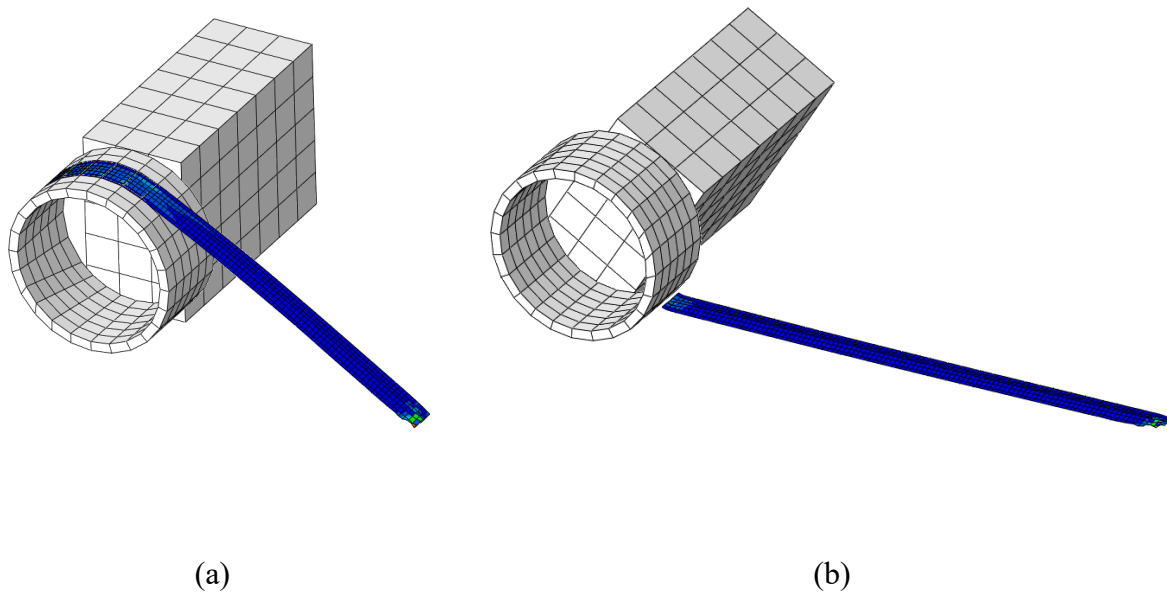


Figure 3: Abaqus CAE Explicit Dynamics model at wrapped state (a) and during deployment (b)

Boundary conditions are placed on the beam to simulate the wrapping simulation and are necessary to properly wrap the beam around the cylindrical hub. The lenticular beam has boundary condition at the tip, preventing the tip from moving in the global y-direction and the bottom edge of the beam from moving in the z-direction. As the hub is rotated about the z-axis, a tensile, axial load is located

at the tip of the beam to allow for the beam to wrap around the hub. Figure 4 and Table 1 below shows where each boundary condition is applied and a description of the constraint/load.

Table 1: Boundary conditions and loads for wrapping and deployment model

Constraint/Load	Description
A	Rotation of Hub purely about Z-Axis for Wrapping
B	Side of beam flange fixed in Z-direction for duration of wrapping
C	Beam tip fixed in Y-direction for duration of wrapping
D	50 lbf shell edge load at Beam Tip

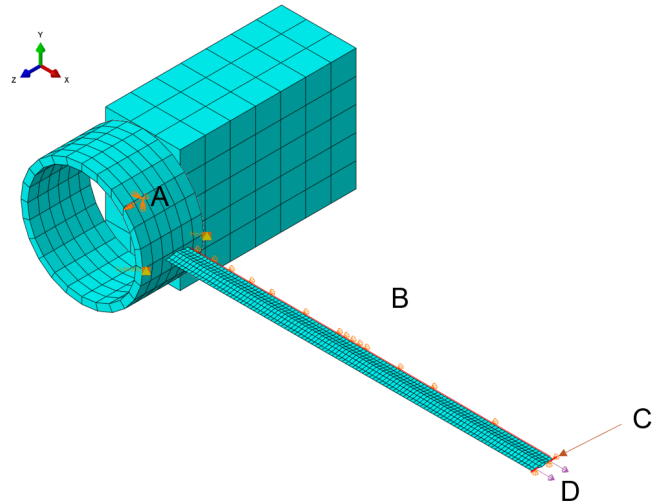


Figure 4: Constraint and load application points for wrapping and deployment model

Simulation time for the wrapping step is 1 second. The maximum transient Hashin damage initiation criteria is measured over this simulation time period. The stored energy at the final time step is taken to be the stored strain energy for the beam. In the subsequent deployment step, the tip load and all other constraints are removed to allow the beam to unfurl and settle over 100 seconds of simulation time. Displacement of the beams outboard-most point in the y-direction will be measured, noting the number of times a change of direction is seen. The average body rotation rates of the assembly during the last 25 seconds of simulation time will also be recovered with the magnitude of the rotation rate about all three axes to be considered in the optimization.

The Abaqus CAE normal modes analysis is used to compute the fundamental frequency of a system with the same beam design parameters, distributed evenly around the hub. The beams are

90 degrees apart and represent the fully deployed structure. The connectors that attach each tube to the central hub in this model are hinge connectors that allow rotation about the global +Z axis of the model. The modes generated are for a free-free system with no boundary conditions or forces acting upon the spacecraft model. The optimizer will use this model to ensure that the first mode of the deployed structure on a spacecraft is above the threshold limit specified.

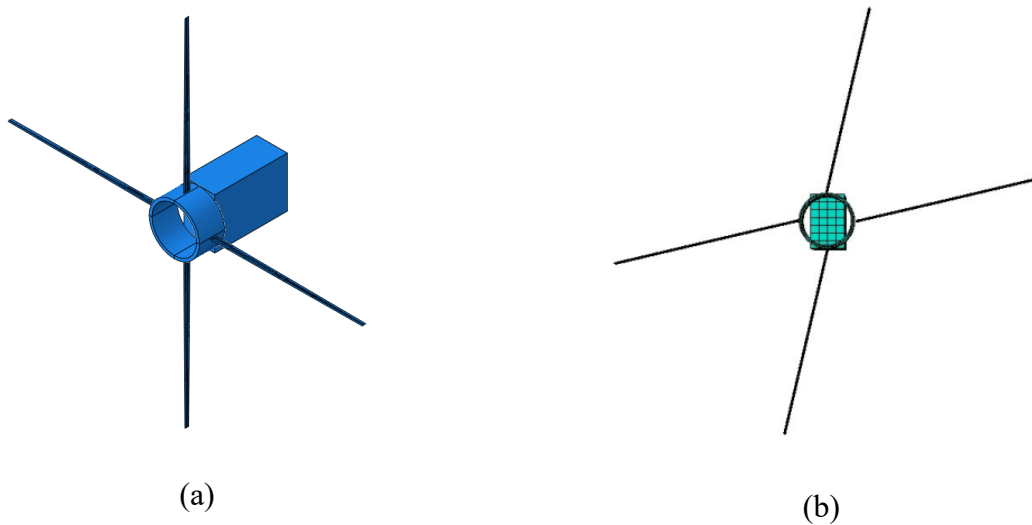


Figure 5: The initial shape for the frequency model (a) and the deformed first mode of frequency (b)

B. Layup Material Property Selection

Helius is a software created by Autodesk that uses micromechanics to simulate and produce material properties for user-defined composites. The software was utilized in previous optimization iterations to produce a table that creates a variety of composite material strength properties for the composite beam makeup. Using the materials library database provided in Helius, the fibers chosen were a fiberglass material, E-Glass, and a carbon fiber material, T300. For the matrix, the low strength option is epoxy 319, and the high strength alternative is epoxy 5505. These materials and their respective material properties can be observed in Table 2 [19], where G_{13} , the out of plane shear modulus is equivalent to the in-plane shear modulus (G_{12}). The

number of plies does not change for each beam design, staying constant at a total of 8 plies that span the lenticular and flange sections of the beam.

Table 2: Material properties chart [19]

Material	E11 (psi)	E22 (psi)	ρ (lb-s2/in4)	G12 (psi)	G23 (psi)	ν
E-Glass	1.05E07	1.05E07	2.434E-04	4.40E06	4.40E06	0.35
T300	3.05E07	2.18E07	1.647E-04	6.53E06	1.02E06	0.35
319	1.38E05	1.38E05	1.191E-04	5.08E04	5.08E05	0.2
5505	1.05E06	1.05E06	1.184E-04	3.89E05	3.89E05	0.2

It is notable that since the E-Glass is a weaved fiber, the Young's modulus in both transverse and axial directions are equal, effectively acting as an isotropic material. However, since T300 is a unidirectional fiber, the Young's modulus varies depending on the orientation of the layup. This introduces the variability of layup combinations, implemented in HEEDS, to allow for composite orientation optimization. In total, 20 different composite materials are generated and read into HEEDS to update material selection for each design iteration. The matrix of combinations and associated strength properties can be referenced in Appendix B. Additionally, it is to be noted that the acquisition of these properties is carried over from previous research and Helius is no longer supported by Autodesk as of February 2022.

C. Optimization

The two Abaqus CAE models are run in the optimization software HEEDS MDO. A python script will generate the material properties and failure strength of a chosen set of layup properties from the matrix of combinations. The algebraic equations for beam root and tip heights, as well as beam weight will also be used to calculate those respective quantities for each design iteration.

Irrespective of being within the optimization constraints at this stage, the design will continue to be run in both frequency and wrapping/deployment models. This is an important distinction in the optimization algorithm compared to previous work as the wrapping and deployment model will run in parallel to the normal modes analysis, i.e., simultaneously. Previous contributions [2, 3, 4] have run both frequency and wrapping models in series disposing of designs that fail the frequency model and not allowing for the wrapping model to be run with those same parameters. The analysis presented in this paper will allow each model to run independent of its feasibility. This will allow the SHERPA optimization algorithm to explore the entirety of the design space more thoroughly, learning from designs that may not fit the constraints of the optimization. Due to computation time, the wrapping & deployment nonlinear simulation is executed in three parallel runs. Siemens sets a standard recommendation of minimum number of evaluations to run the optimization using the SHERPA algorithm. For this optimization, a minimum number of evaluations is determined to be 30 evaluations [20]. However, in favor of the computational power available, a minimum of 100 design evaluations are run. Figure 6 below shows a flowchart describing the overall optimization algorithm architecture.

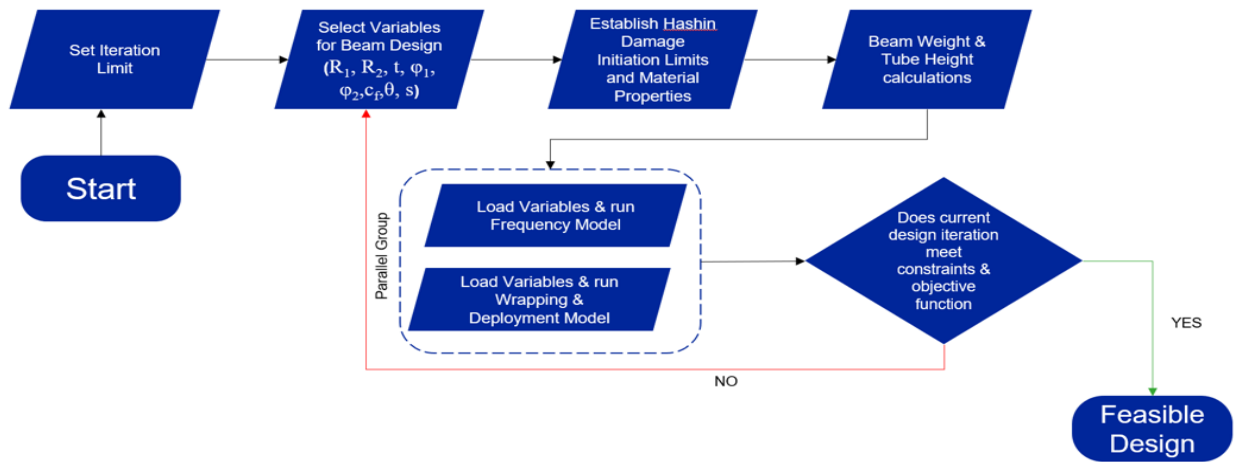


Figure 6: Flowchart of HEEDS Optimization architecture

Table 3 below shows the range of values for HEEDS to select for each parameterized variable and their respective resolution. For the fiber and matrix variables, a discrete set of values were selected based on the material selection possible combinations, hence no resolution is given. The variable “s” is the additional variable added for root-tip taper ratio. A value of 0.2 for “s” represents the most aggressive taper between root-tip. A value of 1.0 for “s” characterizes a beam design that has a constant root-tip cross-section.

Table 3: Optimization Parameter range and resolution

Variable	Range	Resolution
R_1 (in)	1 – 3	0.1
R_2 (in)	1 – 3	0.1
θ (deg)	25 – 65	1
t	0.0014 – 0.015 in	0.0005
c_f	0.45° – 0.65°	0.05
$\phi_{1,2}$	0, 30, 45, 60, 90	15
s	0.2 – 1	0.1
k	0.5 – 3 lbf-in/rad	0.1
d	1 – 5 lbf-in-s/rad	0.1
Fiber	Eglass, T300	-
Matrix	319, 5505	-

The lower bound of ply thickness is taken from the paper published by Thomas Neigh [15]. In his thesis, Neigh lists ply thickness for reference laminates and classifies them as thin, intermediate, and thick. For each ply thickness classification, a corresponding effective Poisson’s ratio is considered. Table 4 below shows the correspondence between the reference laminate classification and effective Poisson’s ratio. This table was used to assess feasible designs from the optimization to determine producibility of a feasible beam design. A script was developed to assess the ply thickness and effective Poisson’s ratio of each feasible beam design from the optimization and designate an indicator value of 0 (unproducibile) or 1 (producibile) to assess producibility. This

producibility factor is not included in the optimization objective function and is only used to contextualize the feasible designs in post processing the optimization results.

Table 4: Feasible Composite Ply Thickness & Corresponding Poisson’s ratio [15]

Ply Thickness Classification	Thickness (in)	ν_{12}
Thin	0.0014	0.314
Intermediate	0.0039	0.274
Thick	0.0118	0.266

IV. Results & Discussion

A. Preliminary Optimization Study

An initial optimization was conducted prior to running the optimization algorithm proposed in this paper. Prior to the implementation of the deployment analysis in the optimization loop, a modified optimization algorithm was run that only included the addition of the root-tip taper ratio for the lenticular beam. The preliminary optimization algorithm still included the modal analysis of a deployed system with tapered beams but only included a dynamic analysis consisting of wrapping the lenticular beam around the central hub. The study was intended to observe the influence of a tapered beam design on wrapping performance and fundamental mode in the deployed configuration. Both the modal analysis and wrapping dynamic analysis were solved quickly in each iteration of the optimization and a large number of designs could be evaluated. The optimization algorithm for this preliminary study is shown in the flowchart of Figure 7 below.

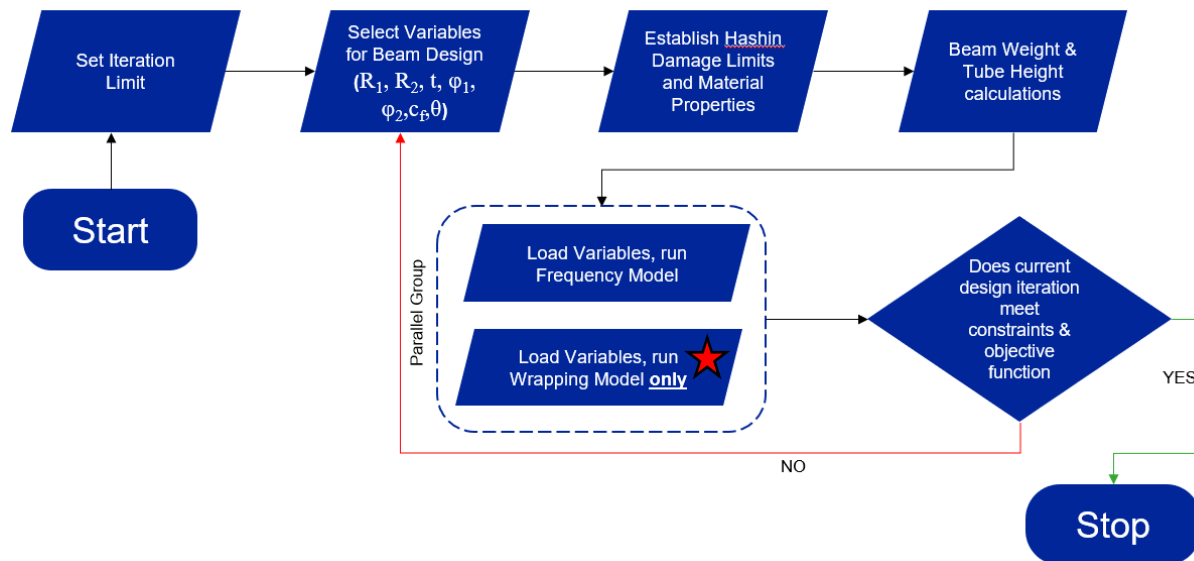


Figure 7: Preliminary optimization algorithm flowchart

The objective function for this optimization also did not include any consideration for deployment behavior. Instead, the design space explored 500 design iterations to find a most feasible design for minimizing strain energy in the beam in its wrapped state and minimizing beam weight. This most feasible design's parameters are shown below in Table 5 and Figure 8 shows the resulting cross-section. The best feasible beam design from this preliminary optimization included a relatively small lenticular opening and an aggressive taper ratio. Though a high taper ratio is included in the best design from this optimization, the influence of the taper ratio seems to be inconclusive as there was no clear correlation between taper ratio and strain energy or beam weight. The ply thickness in this beam design also falls outside of the range of producible laminates. Parameter correlation plots from this preliminary optimization are available in Appendix C.

Table 5: Preliminary Optimization Best Feasible design parameters

Variable	Output
Root R_2 (in)	1.33
Root R_1 (in)	1.25
θ (deg)	28.53
t (in)	0.00075
c_f	0.45
ϕ_1 (deg)	30.00
ϕ_2 (deg)	0.00
Fiber	T300
Matrix	5505
Taper Ratio (s)	0.30

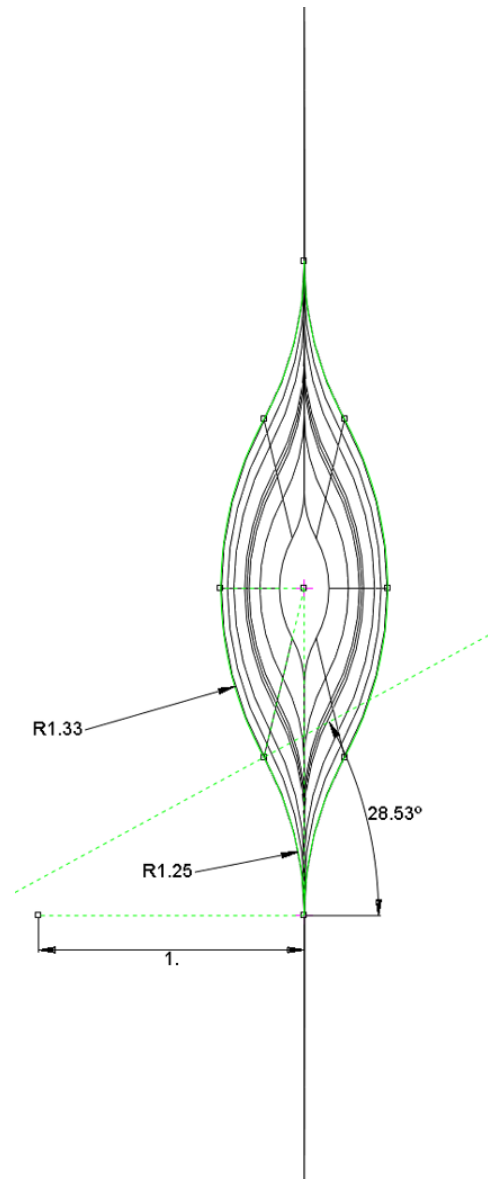


Figure 8: Preliminary Study Best Feasible Root cross-section

The results of this preliminary optimization were useful in determining the input condition that would be used in the main optimization algorithm outlined in Section III. C, Figure 6. The inclusion of the deployment simulation in the optimization loop significantly increases solution time per iteration of the optimization. Therefore, the preliminary study aims to provide an input design close to a potential local optimum to allow SHERPA to explore the local design space

without having to begin the optimization by prioritizing global search. The best design from this preliminary optimization study without beam deployment characteristic consideration may not yield a feasible design for the main optimization algorithm described in Section III. C, Figure 6. However, the intent behind the preliminary study is to allow the SHERPA search algorithm to find a feasible design more quickly than if it had to begin design space exploration from scratch.

B. Optimization Results

The main optimization algorithm was run for nearly 300 evaluations to allow SHERPA to evaluate the design space and find feasible designs per the objective function and constraints described in the previous sections. The preliminary study was used to provide a starting point for the search algorithm in this main optimization. The performance of feasible designs will be discussed further detail in this section, focusing on the correlation between objective function variables and correlation between design parameters. Impact of the additional design parameter “*s*” to produce a chordwise beam taper will also be discussed this this section. Influence charts using Boruta and Sobol index calculations will help strengthen these correlations to determine which input variables have direct impact on simulation outputs. The added context of producibility in the feasible designs gathered from the optimization will also be discussed in this section.

1. Best Feasible Beam Design

Of nearly 300 designs evaluated, 105 designs were deemed feasible according to the constraints set, and all data plots shown will pertain to those 105 feasible designs. The differences between the input design and the best feasible design found by the optimization can be seen in Table 6, with the cross-section shown in Figure 9. Compared to the input design, the best design found by the optimization shows large changes in strain energy and weight. Geometrically, the cross-section

dimensions are larger than the input, which equates to a larger beam footprint. The lenticular opening is very similar, however, with both designs being on the lower end of the Root θ range. The ply thickness is also thicker, which equates to the mass of the best feasible beam being heavier. However, the fiber and matrix chosen by the optimization is the same when compared to the input condition. Taper ratio is also significantly different with the optimization's best design favoring a higher value that equates to a more uniform cross-section along the length of the beam, i.e., a less aggressive taper.

Table 6: Main Optimization Best Feasible Design Parameters

Parameter Name	Input	Main Optimization Best Feasible Design	% Change
Weight (lb)	0.13	0.42	225%
Strain Energy (lbf-in)	1.03	9.60	834%
Frequency (Hz)	0.61	1.00	63%
Fiber Tension	0.02	0.02	32%
Fiber Compression	0.02	0.05	133%
Matrix Tension	0.44	0.15	67%
Matrix Compression	0.07	0.03	60%
Root Height (in)	4.57	6.28	37%
Body Rotation Rate (deg/s)	-	0.02	-
Tip Displacement Peaks	-	1.00	-
Ply Thickness (in)	7.50E-04	1.40E-03	87%
R ₂ Root (in)	1.33	3.00	125%
Root θ (deg)	28.53	25.00	12%
R ₁ Root (in)	1.25	1.90	52%
Taper Ratio, s	0.30	0.78	164%
Fiber Index	T300	T300	0%
Matrix Index	5505	5505	0%

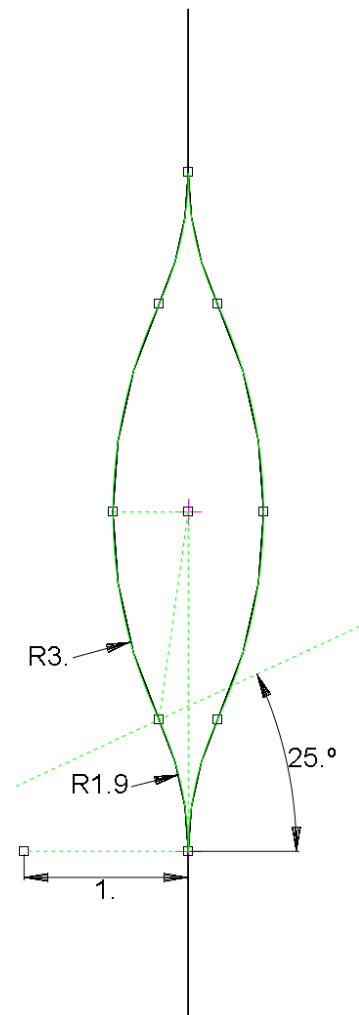


Figure 9: Best Feasible design from the Main Optimization

2. Objective Function Parameter Correlation

The objective functions for this optimization involved the weight, stored strain energy in the wrapped state and tip displacements during deployment. The correlation between these three variables is seen in Figure 10 (a)-(c) for all feasible designs produced by the optimization. Figure 10 (a) shows a clear positive correlation between beam weight and stored strain energy in the wrapped state. This is likely due to the weight being heavily influenced by ply thickness, which will be a reoccurring theme in subsequent sections. A beam with thicker plies will develop more strain, which is what is seen in the relation between weight and strain energy. Since the stored strain energy and beam weight are positively correlated and minimized equally, a change in the design will usually either benefit both or detract from these two variables. Clustering is seen in the feasible designs of Figure 10 (b) and (c) in which designs with less weight and less strain show less oscillatory behavior upon deployment. Designs with a weight close to 0.5 lbs see less strain develop, and these designs tend to see less than 10 beam tip displacements, with many of them having less than 5. While there exists a similar cluster in the beam displacements at weight of 0.5 lbs, both Figure 10 (b) and (c) see a spread near their respective clusters, which could be due to the inherent unpredictable nature of the beam's unfurling. Most notably, the clustering of these feasible designs is indicative that the optimization has found a local minimum in the design space. The designs being found adhere to the objective function's aim to minimize the three objective components and each feasible design can do so within the constraints established. The deployment oscillations seeing more spread could also be the result of the SHERPA global search method which explores further from local search area in hopes to find another local optimum, inferring that other local optimums may exist within the design space.

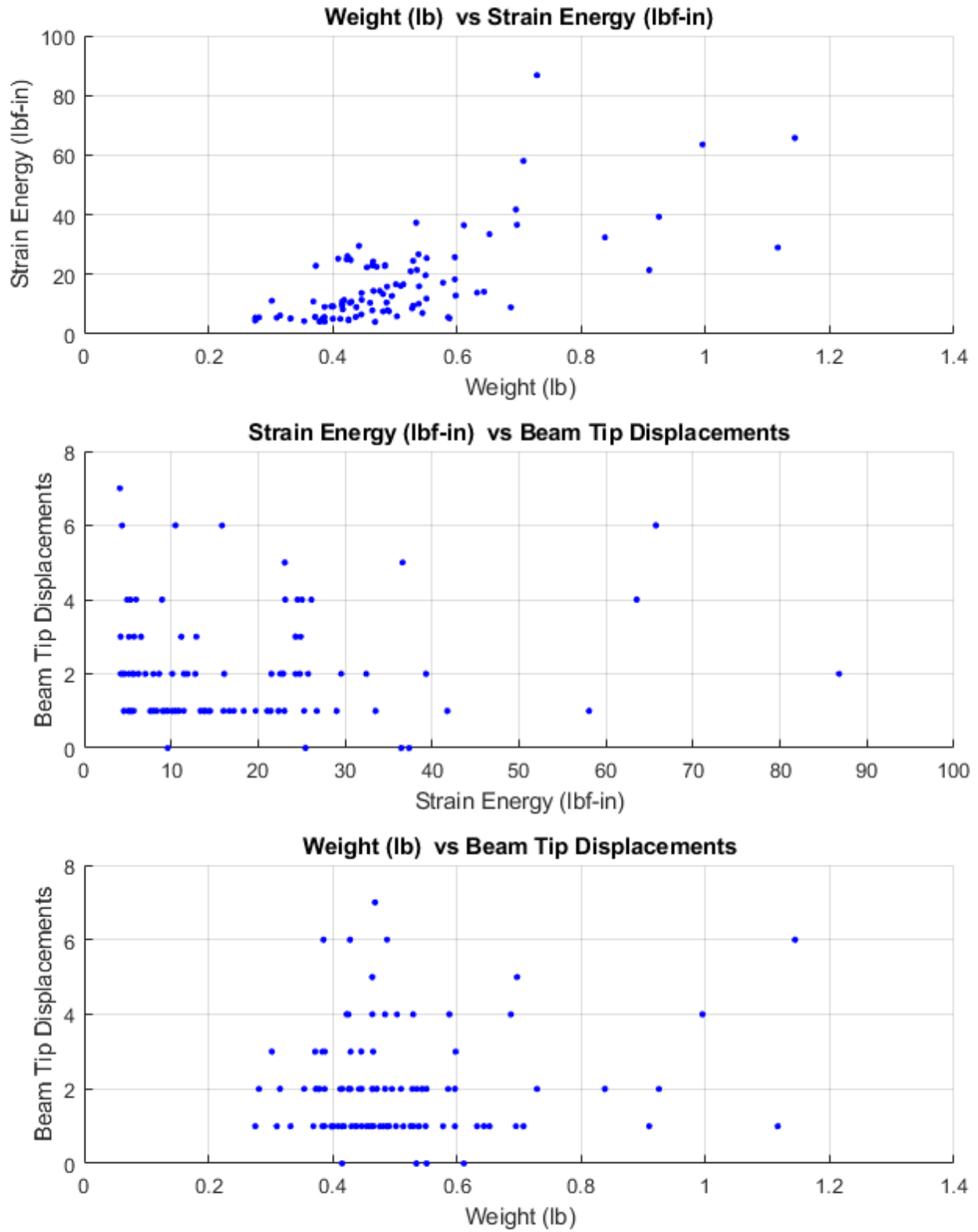


Figure 10: Objective Function Correlations for Weight vs Strain Energy (a), Strain Energy vs Beam Tip Displacements (b), Weight vs Beam Tip Displacements (c).

3. Input/Output Parameter Correlation

The influence of certain input variables can impact the output variables of interest. In this optimization effort, the addition of a chordwise taper has been introduced to understand the tapered beam's influence on output parameters like stored strain energy in the wrapped state and deployment characteristics. Figure 11 (a) shows that there exists a strong correlation between beam weight and the taper ratio. A taper ratio having a more consistent cross-section (closer to 1.0) will have a larger cross-sectional area and thus more volume, which inherently leads to more weight of the beam. Clustering is also present in the feasible designs at the higher end of the taper ratio range. Nearly 90 % of feasible designs have a taper ratio higher than 0.6, indicating feasible designs found by the optimization tend to be of a less aggressive taper closer to a value of 1.0. Figure 11 (b) shows that a taper ratio of 0.6 or higher see less strain energy develop in the beam and Figure 11 (d) shows that these beams deploy with less body rotation imparted on the system. Displacement peaks see a larger spread in the taper ratio region from 0.6 to 1.0. This spread, seen in Figure 11 (e) is similar to the objective correlation between stored strain energy and oscillatory behavior, and so it is difficult to directly correlate taper ratio to oscillatory behavior of the beam. What can be said, however, is that the linear relation between taper ratio and weight of the beam juxtaposes the taper ratios influence on strain energy. Clearly, a balance must be struck for the beams taper ratio as the optimization minimizes weight and strain energy. Additionally, it can be shown that the optimization tends to prefer a taper ratio closer to a value of 1.0 for the data presented.

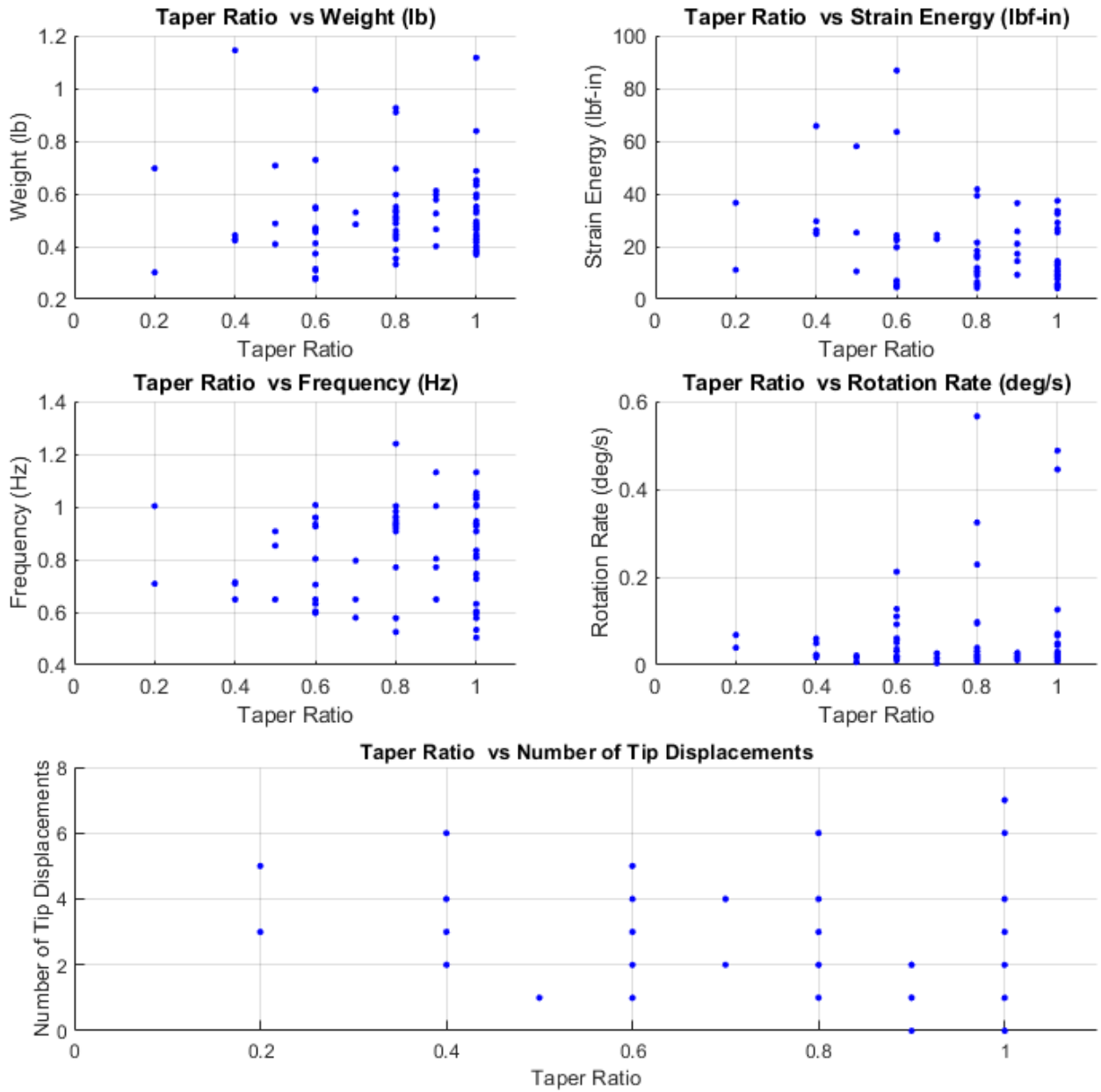


Figure 11: Parameter Correlation for Taper Ratio vs Weight (a), Strain Energy (b), Frequency (c), Rotation Rate (d), Tip Displacements (e).

Other input and output variable correlations have also been analyzed. However, due to the nature of the optimization, and the fact that input parameters are not held constant as the optimization explores the design space, correlation may prove to be inconclusive at times. The next input variable correlation to observe is laminate ply thickness of a beam design. Here, a strong linear correlation exists between ply thickness and beam weight as shown in Figure 12 (a). This linear relation inherently makes sense, as mentioned previously, when taking into consideration the formula for beam weight. An increase in the ply thickness will proportionally increase the weight of the beam based on Equation (2). Figure 12 (b) also shows strong correlation between strain energy stored in the beam and ply thickness. The ply thickness has a direct impact on stiffness of the beam and such, strain energy developed when wrapping the beam will increase with a thicker beam. This stiffness consideration is also present in the linear relation seen between ply thickness and fundamental frequency of the beam shown in Figure 12 (c). A thicker ply will lead to a deployed system with stiffer beams and a higher fundamental mode. The relation between ply thickness and deployment characteristics is less clear, however. There exists a large spread in the oscillatory behavior of the beam despite changing ply thickness and the small amount of clustering happening at the lower end of the ply thickness range in relation to rotation rate imparted is not significant enough to draw any clear relations. Overall, the ply thickness relations observed are consistent with the understanding between material ply thickness and the beam's overall stiffness.

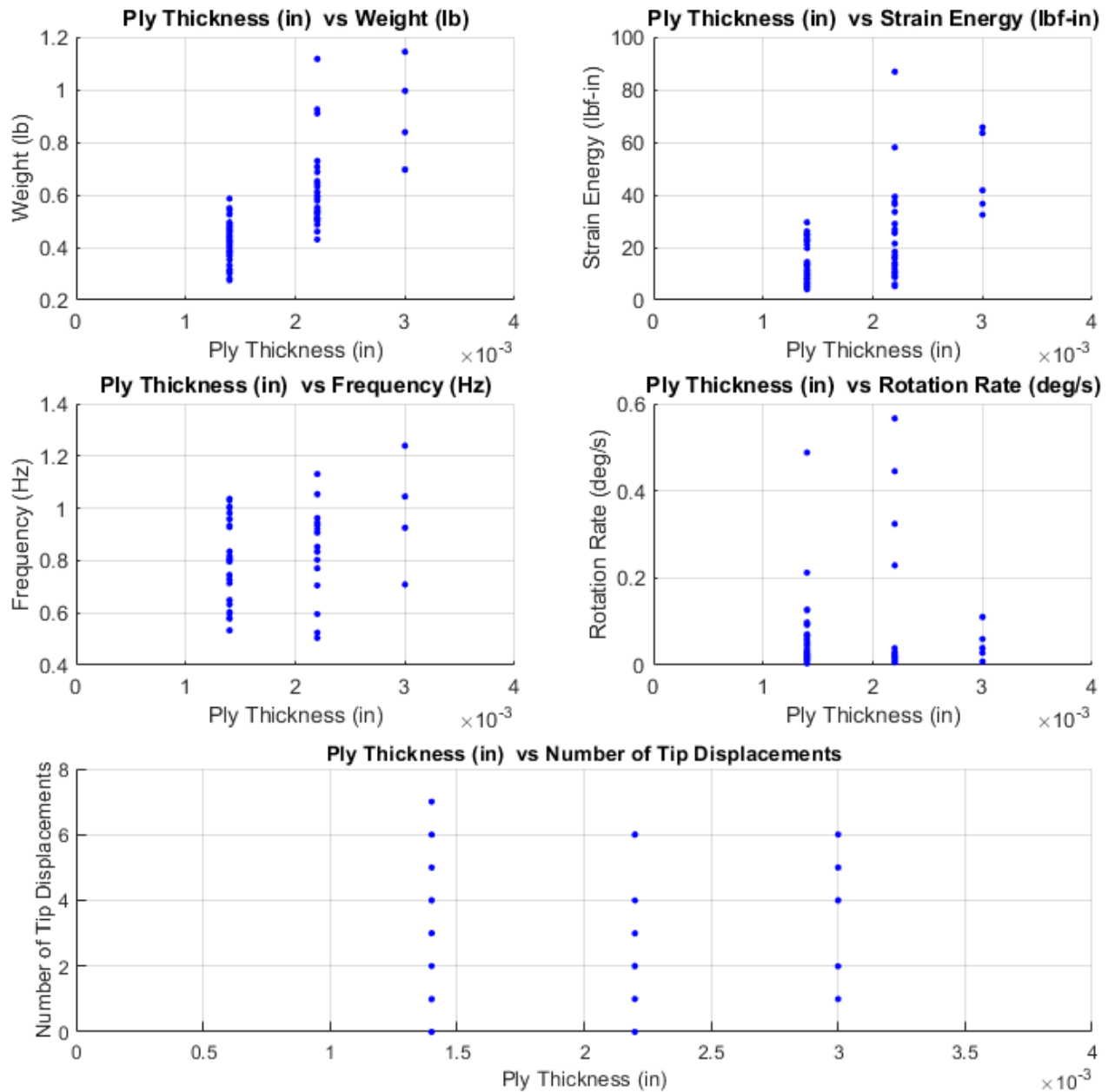


Figure 12: Parameter Correlation for Ply Thickness vs Weight (a), Strain Energy (b), Frequency (c), Rotation Rate (d), Tip Displacements (e).

The Root θ input parameter is the main driver in determining how large the lenticular opening of the beam will be. A larger value will equate to a larger opening, and vice versa for a smaller value of Root θ . As the beam is wrapped, it must close the lenticular opening, causing strain energy to develop in the beam. Though no clear correlations can be seen in the plots of Figure 13, what is of note is the clustering that is happening in each plot. The feasible designs seemingly cluster at the lower range of Root θ , between 20 and 40 degrees. This leads to the notion that the optimization prefers designs that have a smaller lenticular opening to best meet the objective function and constraints. Designs with lower Root θ values tend to also have lower strain energy and similarly have a smaller rotation rate imparted on the system upon deployment, as seen in Figure 13 (b) and (d). The relation between strain energy and Root θ is consistent with the understanding that a smaller lenticular opening will develop less strain as it deforms. This viscoelastic behavior is well documented, and it carries over to the results of this optimization. Deployment displacement peaks have a larger spread, especially around the 25- and 35-degree values, once again making it hard to correlate oscillatory nature of the deployment to this parameter, suggesting that tip displacements are not solely depending on the beam's Root θ value. Overall, feasible designs from this optimization consist mostly of cross-sections with smaller lenticular openings at a rate of 92% of design with lower than 45-degree Root θ value.

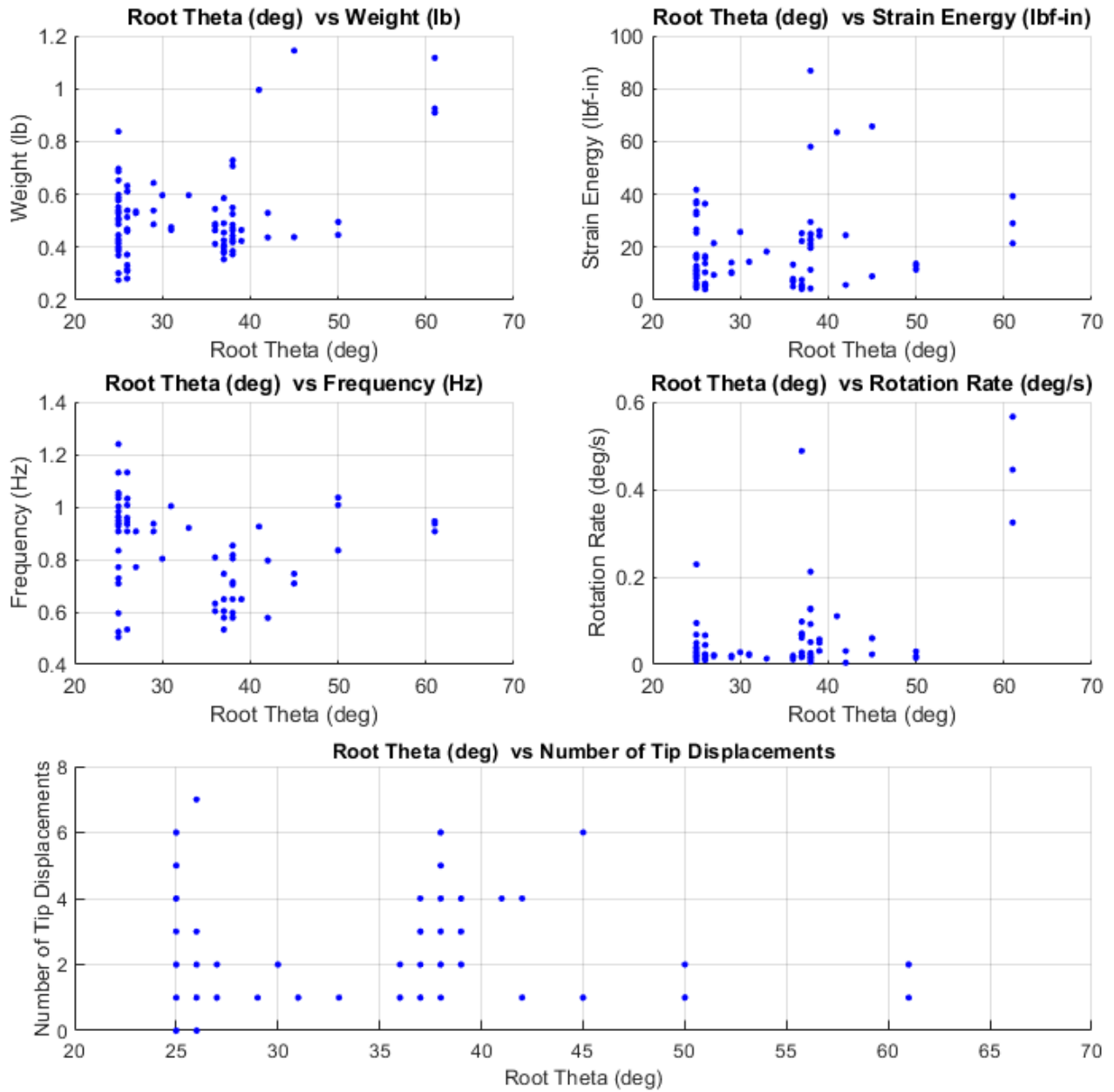


Figure 13: Parameter Correlation Root θ vs Weight (a), Strain Energy (b), Frequency (c), Rotation Rate (d), Tip Displacements (e).

Fiber orientation for the composite layup of the beam is also looked, particularly the inside and outside plies. Figures 14 and 15 below show the parameter correlation between interior and exterior ply fiber orientation, Φ_1 and Φ_2 , respectfully. Interior fibers refer to the fibers that are sandwiched by the exterior fibers on the outer portion of the beam and within the lenticular section. Exterior fibers will either make contact with the hub or make contact between themselves in the lenticular portion of the beam. For interior fibers in Figure 15, clustering of feasible designs containing a fiber orientation of 0 or 30 degrees is seen, with exterior fibers in Figure 14 having a larger spread in their orientation angle. These quantities are a bit harder to justify in 2D correlations since the combination of both fiber orientation angles will affect the output variable. Since the ply orientation is never fixed for either interior or exterior fibers. What we can see is that the interior and exterior fibers see a slight linear correlation for orientation angle and strain energy. This tells us that a composite layup that includes interior and exterior fibers, especially those that are unidirectional like T300, will see higher strain energy develop. This is precisely what can be seen from Figure 14 and 15 (b). This should intuitively make sense as an orientation angle greater than 0 will cause a composite layup to become stiffer in some cases and generate more strain energy as it deforms. As the orientation angle moves from 0 or 90 degrees, the fundamental frequency should go up. This is seen in Figure 14 (c) and Figure 15 (c) as clustering of designs with high fundamental modes predominantly being at the 30- or 60-degree configuration. However, the connection of fiber orientation to deployment characteristics is less clear as the spread is quite large in the data, leading to the notion that fiber orientation may not significantly affect deployment behavior of the beam.

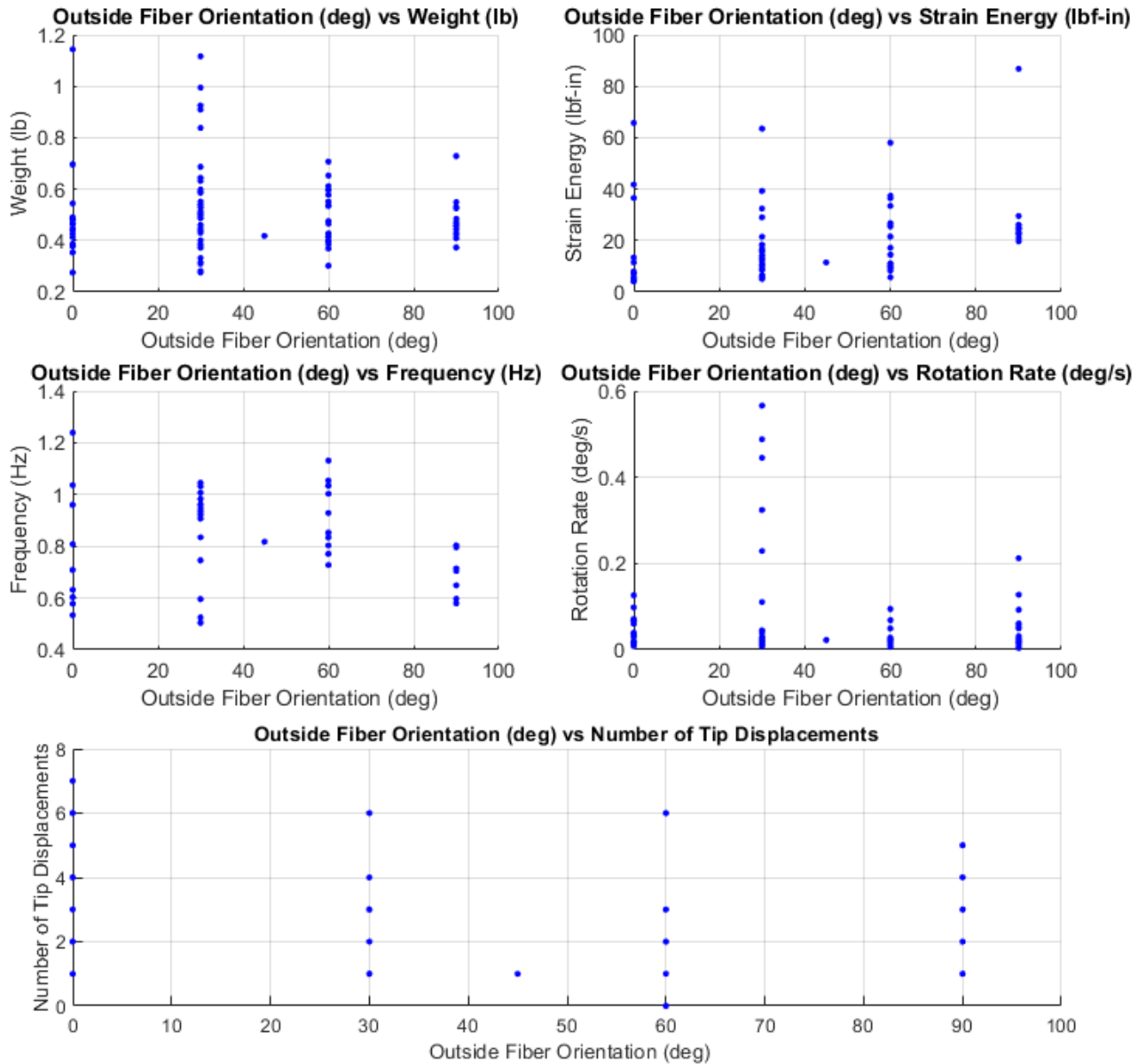


Figure 14: Parameter Correlation of Outside Fiber Orientation vs Weight (a), Strain Energy (b), Frequency (c), Rotation Rate (d), Tip Displacements (e).

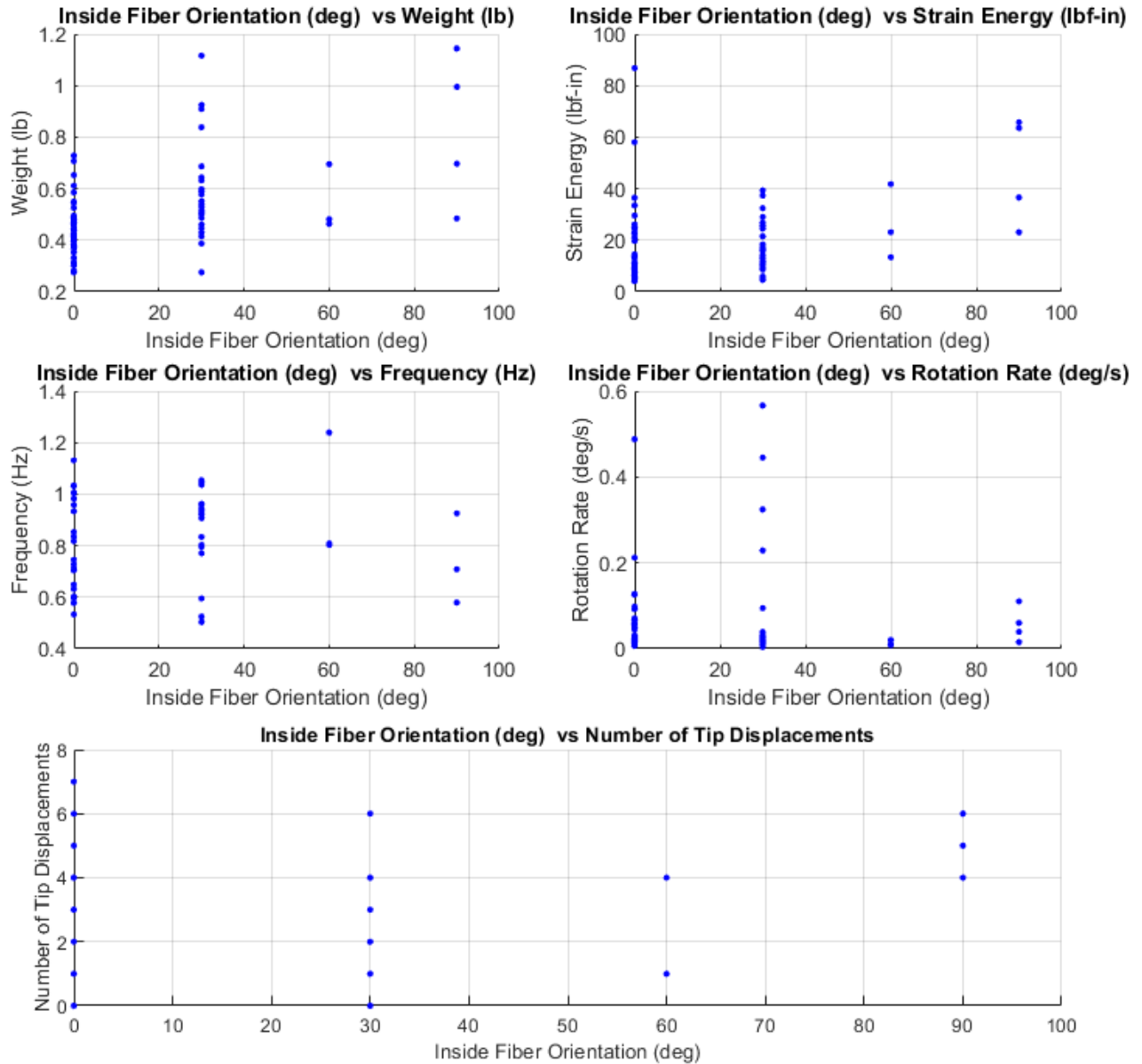


Figure 15: Parameter Correlation of Inside Fiber Orientation vs Weight (a), Strain Energy (b), Frequency (c), Rotation Rate (d), Tip Displacements (e).

Material selection by the optimization algorithm and the correlation of these materials to the tracked output parameters. Matrix and Fiber are chosen by the optimization in its design exploration, pulling from a list of pre-determined material combinations, as described in Section III. B. Matrix selection is largely well distributed between the two options, 5505 and 319, with no one matrix being overly dominant, as seen in Figure 16. Of note, matrix 5505 develops less strain and less oscillatory behavior, but can induce slightly more rotation onto the system upon deployment than matrix 319. Additionally, matrix 319 has a lower fundamental mode than 5505, leading to the notion that 5505 is stiffer and may be better suited for the beams on-orbit vibrational characteristics. This is proven when looking into the Young's modulus of the 5505 matrix, noted in Table 2. As for fiber selection, the optimization overwhelmingly deems T300 fiber to be the better of the two selectable fibers. Feasible designs from the optimization do not consider E-glass fiber to be suitable for the wrapping and deployment characteristic of the beam, given the constraints. Though there are only two available choices for fiber input, the designs that use T300 fiber are best suited for this optimization's constraints and objective. Future iterations of this optimization study could implement a larger selection of fibers and matrices to see if the correlations shown remain relevant.

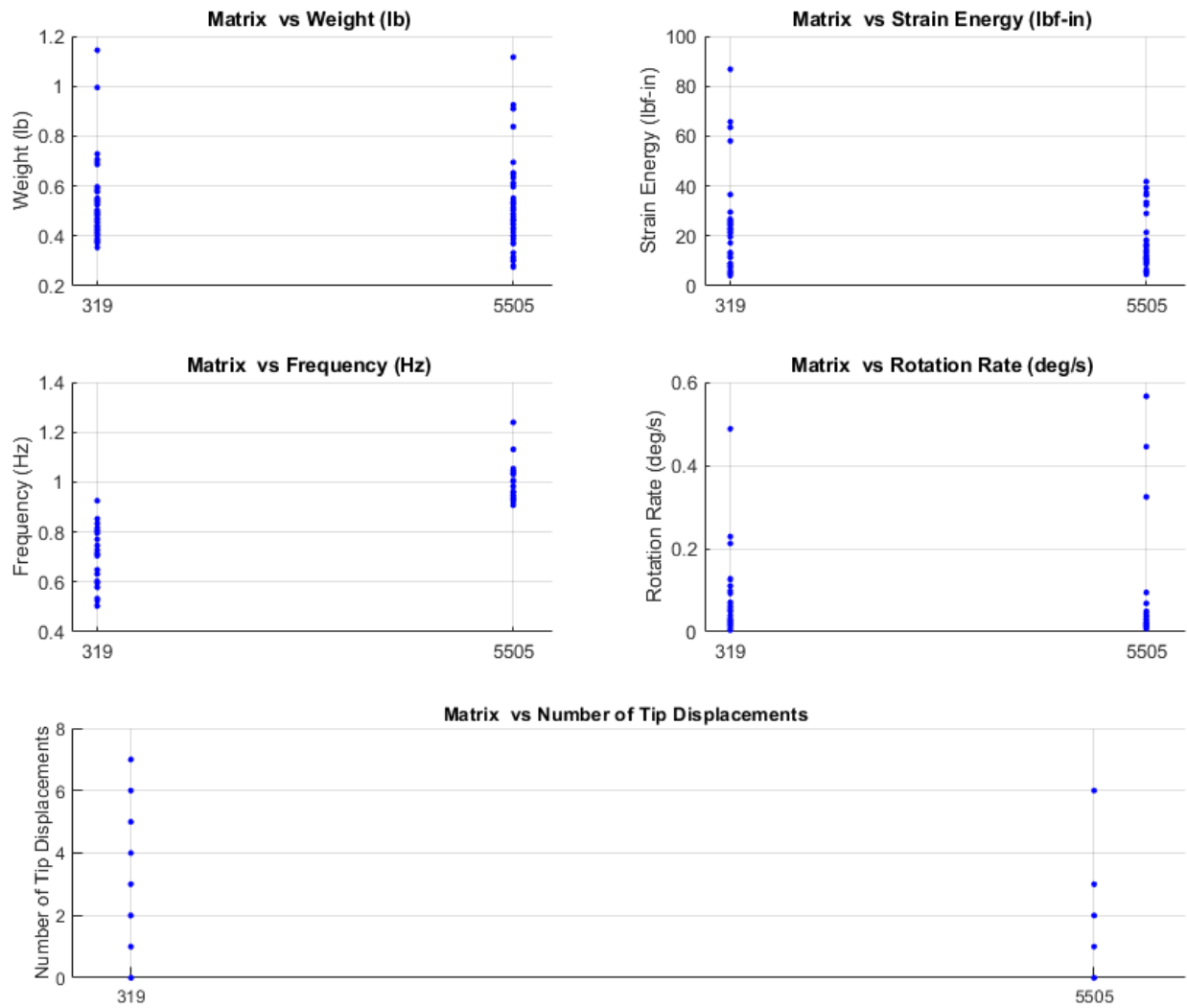


Figure 16: Parameter Correlation of Matrix Selection vs Weight (a), Strain Energy (b), Frequency (c), Rotation Rate (d), Tip Displacements (e).

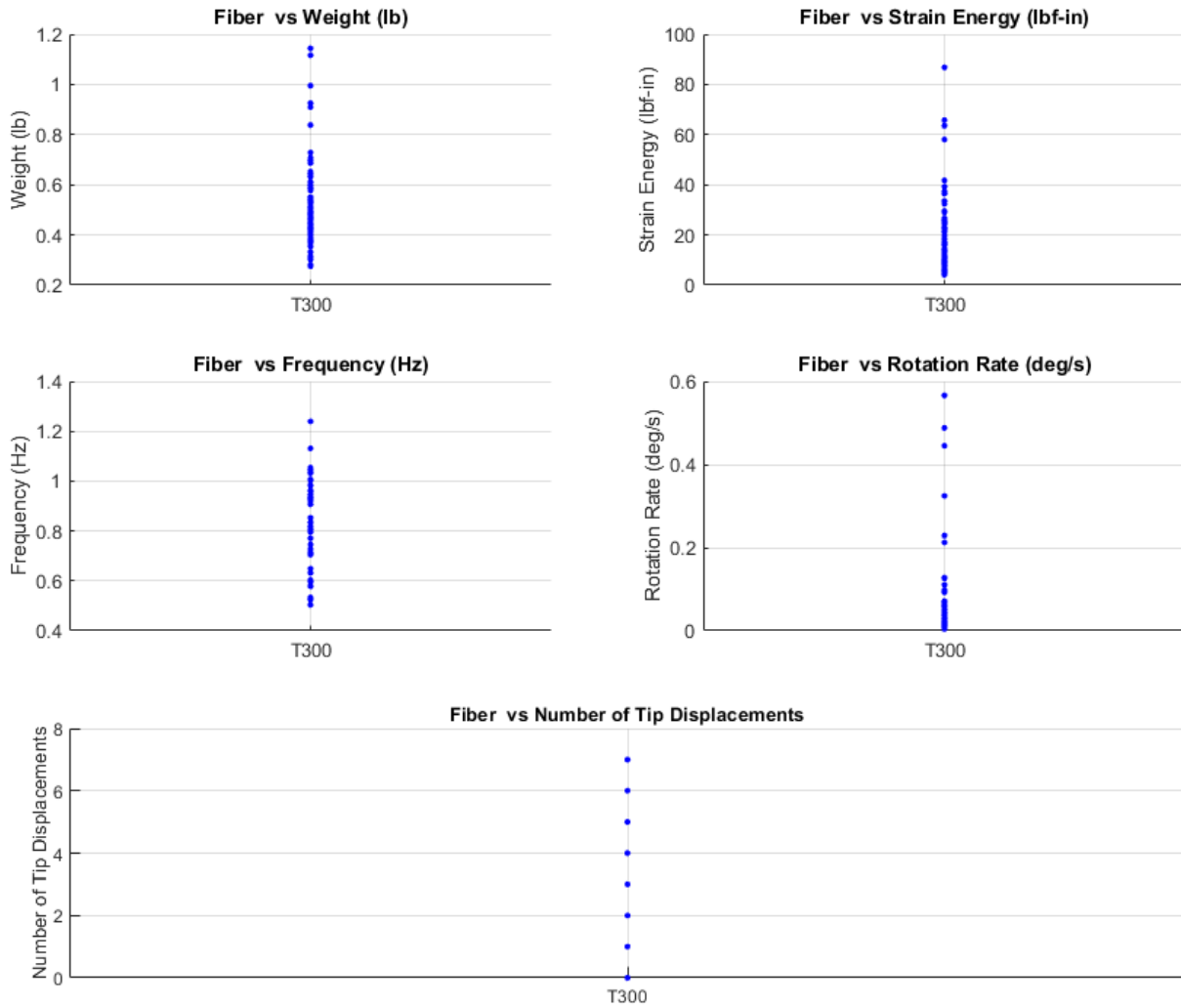


Figure 17: Parameter Correlation of Fiber Selection vs Weight (a), Strain Energy (b), Frequency (c), Rotation Rate (d), Tip Displacements (e).

Lastly, the correlation between stiffness and damping at the boundary conditions between the composite beam and the rigid central cylinder is observed. Both inputs, boundary stiffness and damping, should have an effect on the deployment characteristics of the beam as they directly influence how much rotation the beam will see when released and allowed to unfurl. Figure 18 shows the correlation between boundary condition stiffness and the outputs of interest, with clustering seen between 0.5 and 1 lbf-in/rad. This shows that most designs tend to prefer a lower boundary stiffness. This makes intuitive sense as the optimization will naturally try to minimize the amount of energy released upon deployment, and a primary source will be from the boundary. Figure 18 (d) shows that body rotation of the system does not seem sensitive to boundary stiffness as there is an even spread in the data. Figure 18 (e) shows a stronger linear correlation with a higher stiffness at the boundary equating to designs that show more tip displacements, agreeing with the notion that less stiffness in the boundary connection leads to less tip displacements.

Figure 19 focuses on the boundary condition damping, showing a similar clustering around the 2.6 lbf-in-s/rad value. Though clustering is seen around this value, correlations between the beam displacement characteristics is difficult to discern. Damping value seemingly stays in the same region, with limited spread of other damping values. Interestingly, damping values see a wide range of tip displacements in Figure 19 (e). This could indicate that the boundary condition damping does not influence tip displacements directly. This is plausible as the beam can deform as it unfurls. There also exist radial stops on the hinge and cylindrical joints that attach the beam to the cylinder which could be causing the beam to bend about the boundary and allows the tip to deflect beyond the neutral position despite and cause displacements to increase due to local deformation.

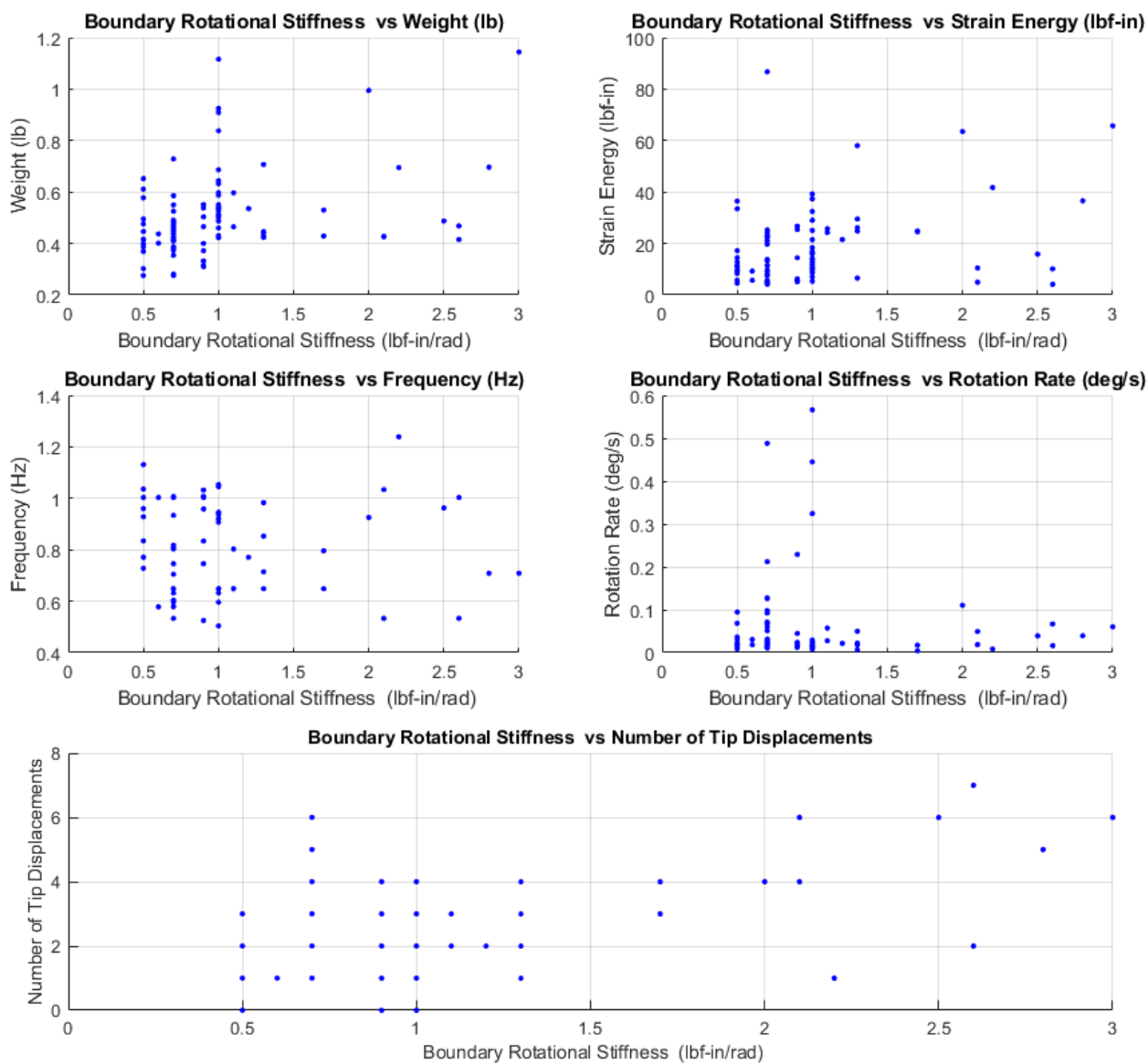


Figure 18: Parameter Correlation of Boundary Stiffness vs Weight (a), Strain Energy (b), Frequency (c), Rotation Rate (d), Tip Displacements (e).

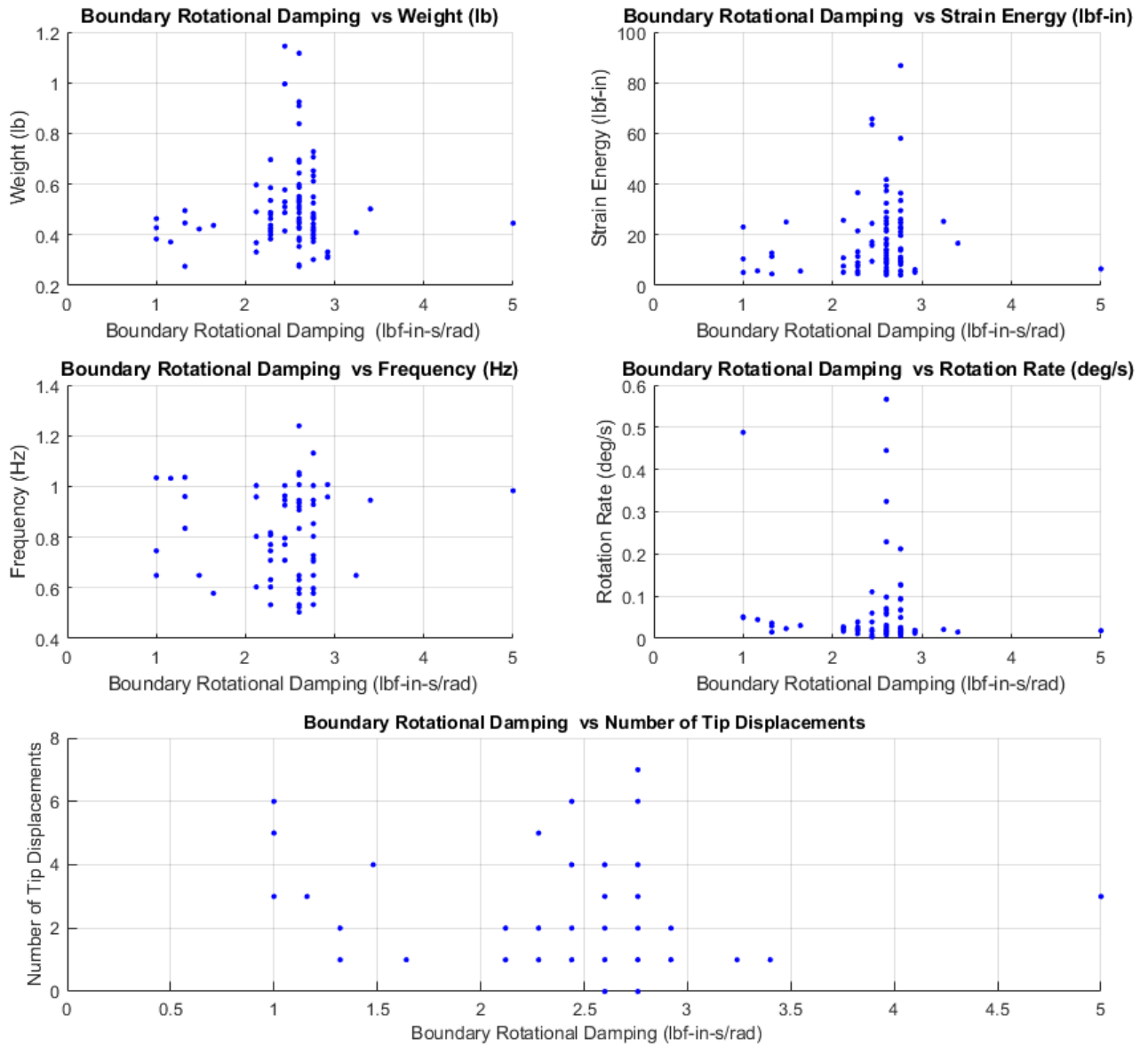


Figure 19: Parameter Correlation of Boundary Damping vs Weight (a), Strain Energy (b), Frequency (c), Rotation Rate (d), Tip Displacements (e).

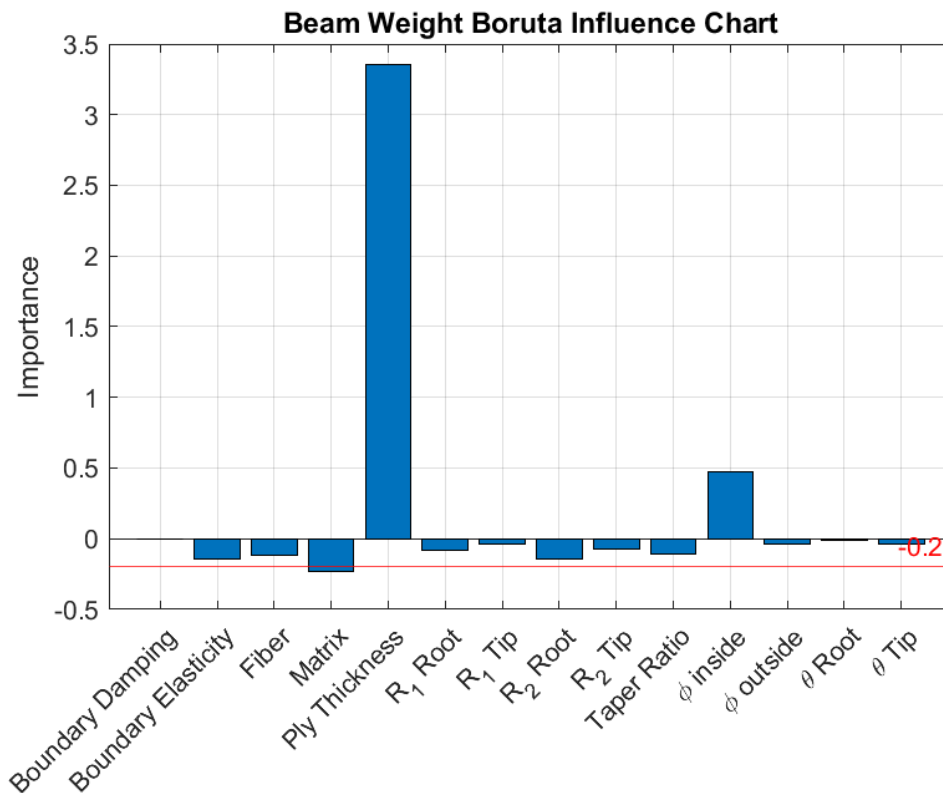
4. Influence Charts

Influence charts are another helpful tool to investigate the relationship between optimization input parameters and outputs of a beam designs' wrapping and deployment performance. One type of influence chart discussed will use the Boruta feature selection method to determine importance of a particular feature or input. Boruta determines an influence threshold, and if a variable has an importance value higher than this threshold it is deemed important. Otherwise, the algorithm categorizes the variable as unimportant. This algorithm is heuristic in nature and is based on trial and error methodology. This means that while influence charts using the Boruta calculation can be helpful in giving insight on the performance of the optimization, we cannot rely on them as they do not guarantee a relation between the simulation outputs and influential variables [21]. However, we can utilize these charts to help us better understand input and output relationships in conjunction with the 2-D correlations observed in the previous section.

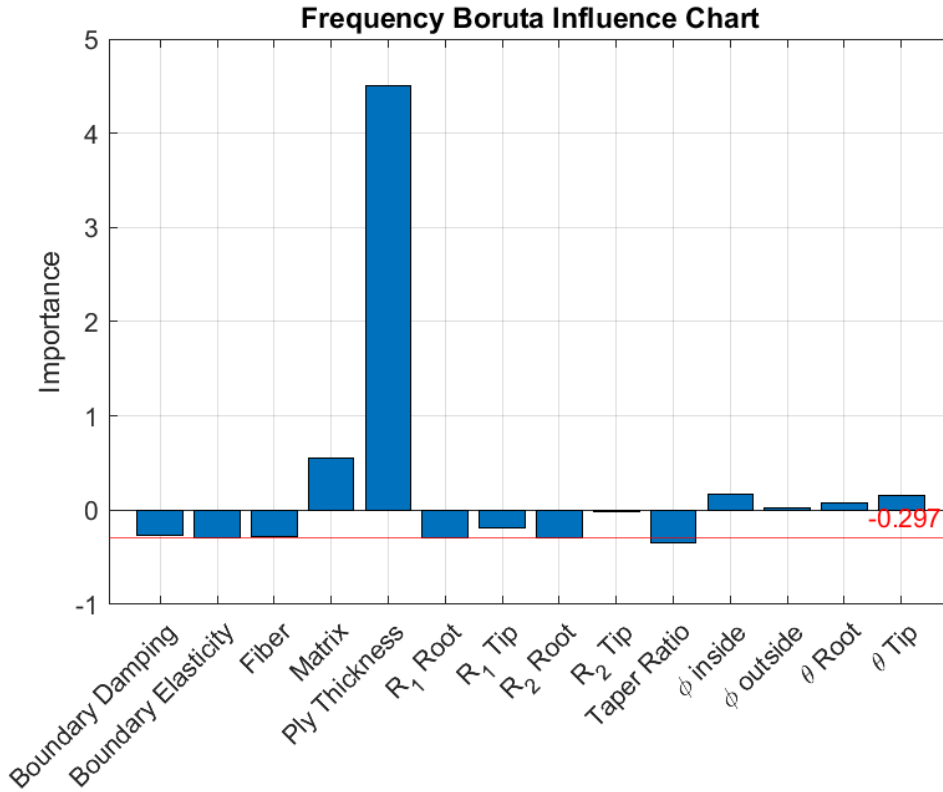
The Sobol Index is also computed to assess relative importance and sensitivity between input and output parameters [22]. The Sobol Index method uses variance decomposition of the response variable to determine the sensitivity of a myriad of input variables, denoting them as significant if the variable's index is above a chosen influence threshold. Influence charts shown from this optimization are calculated using the HEEDS MDO post processing suite, which uses the optimization design data to produce plots using the Boruta and Sobol algorithm.

Figure 20 (a) shows the influence of input parameters on the weight of the beam from the optimization. The weight's main influence stems from the ply thickness of the beam. This intuitively makes sense as the thickness is strongly correlated with beam weights, as we discussed in the previous sections. Ply thickness of the composite beam will influence the overall volume of the design, hence increasing weight. The previous section also discussed this interaction between

thickness of the beam and its influence on overall stiffness of the structure, and the relationship is carried over here. Figure 20 (b) shows fundamental frequency of the beam in its deployed configuration to be heavily influenced by the composite ply thickness. It should be noted that the importance threshold for both outputs in Figure 20 (a) and (b) show relatively low values. This means that there is a high probability of many variables considered to be influential to weight and fundamental frequency of the beam. However, the thickness input parameter is proportionally higher than other parameters, establishing its influence on these outputs. Ultimately, the strong linear correlation seen in ply thickness vs weight and deployed frequency of a beam design in prior sections is reiterated in both influence charts.



(a)



(b)

Figure 20: Boruta Influence Chart for Beam Weight (a) and Fundamental Frequency (b).

Geometric parameters largely influence the stored strain energy of the beam in its wrapped state. The largest influence on stored strain energy is coming from the lenticular curvature parameter R_1 , particularly in the root cross-section. Other root and tip cross-sectional parameters, as well as the ply thickness, also show influence on stored strain energy. However, these inputs do not break the importance threshold. This influence chart’s results are not unexpected as the influence of stored strain energy in the beam is likely to be due to the viscoelastic behavior of the beam’s lenticular shape. This is clearly seen in this influence chart as cross-sectional input parameters have the highest importance values. Sobol plots for Beam Weight, Fundamental Frequency and Strain energy report similar conclusion as those discussed for their Boruta counterparts and are referenced in Appendix D.

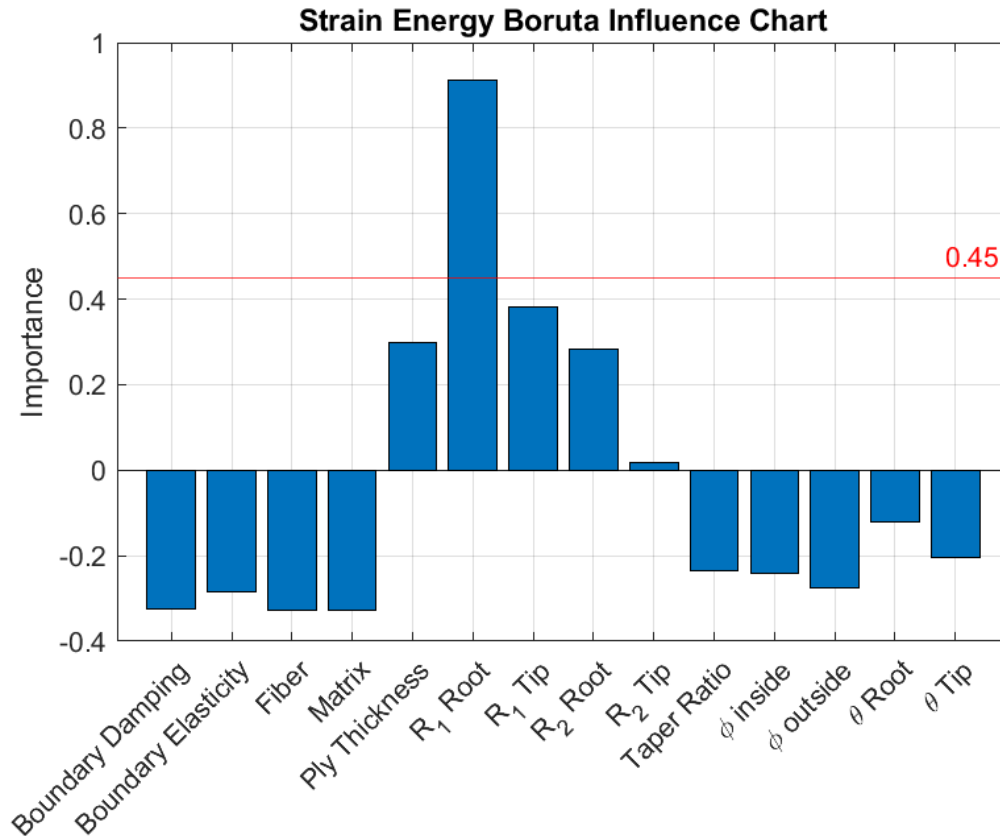
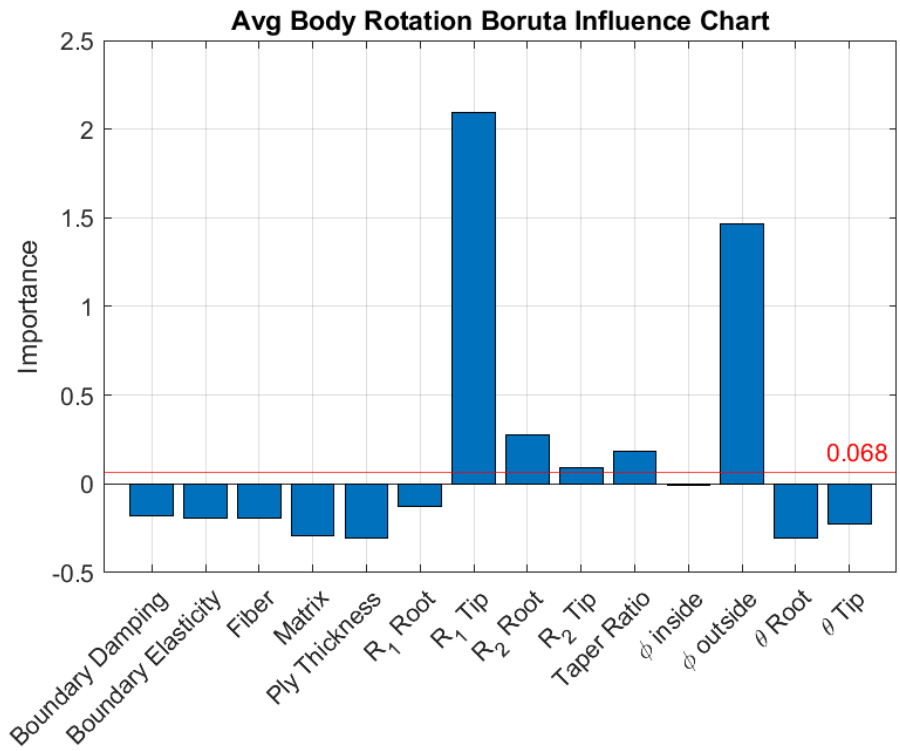
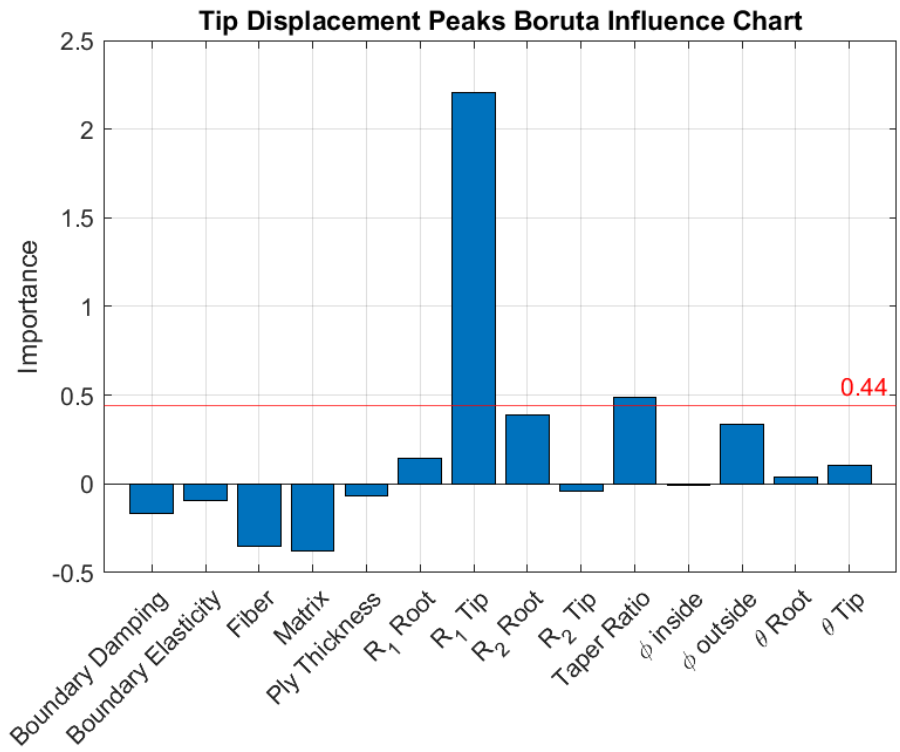


Figure 21: Boruta Influence Chart for Beam Stored Strain Energy.

Lastly, influence charts for the deployment characteristics of the beam will be analyzed. Boruta influence charts for these output responses in Figure 22 (a) and (b) show large importance values for beam cross-sectional values, such as R_1 and R_2 for both root and tip. This high importance values for these parameters could be due to the nature of the unfurling of the beam. Since the boundary connections have rotation limits, the beam could be rotating about the boundary. This could lead to the beam's overall cross-section and resulting inertial characteristics to determine how the oscillatory behavior of the beam is, as well as how much rotation is imparted on the system. Taper Ratio of the beam also sees high importance, also contributing to the notion that cross-section parameters are of high importance for deployment characteristics.



(a)

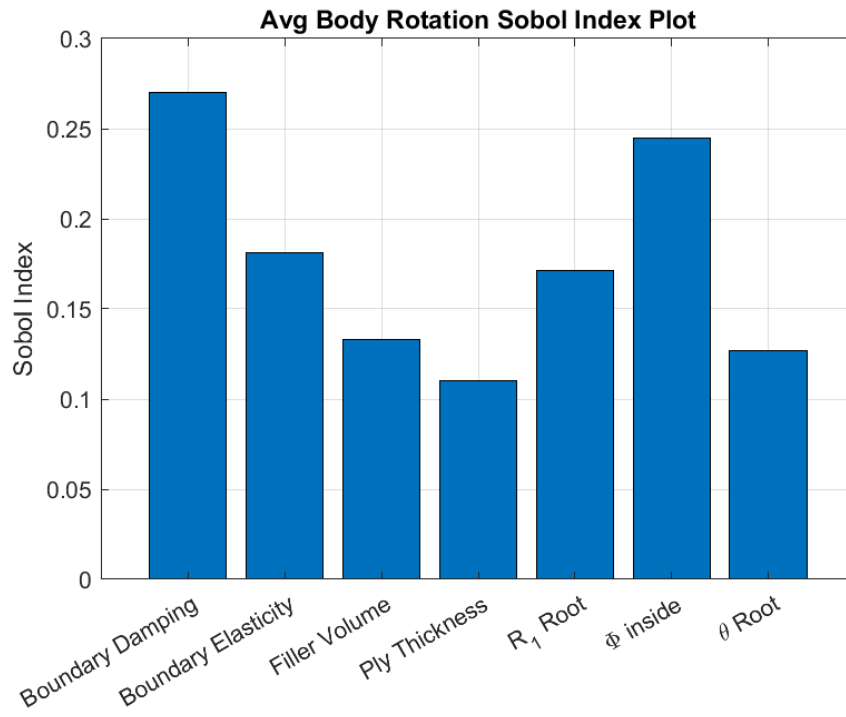


(b)

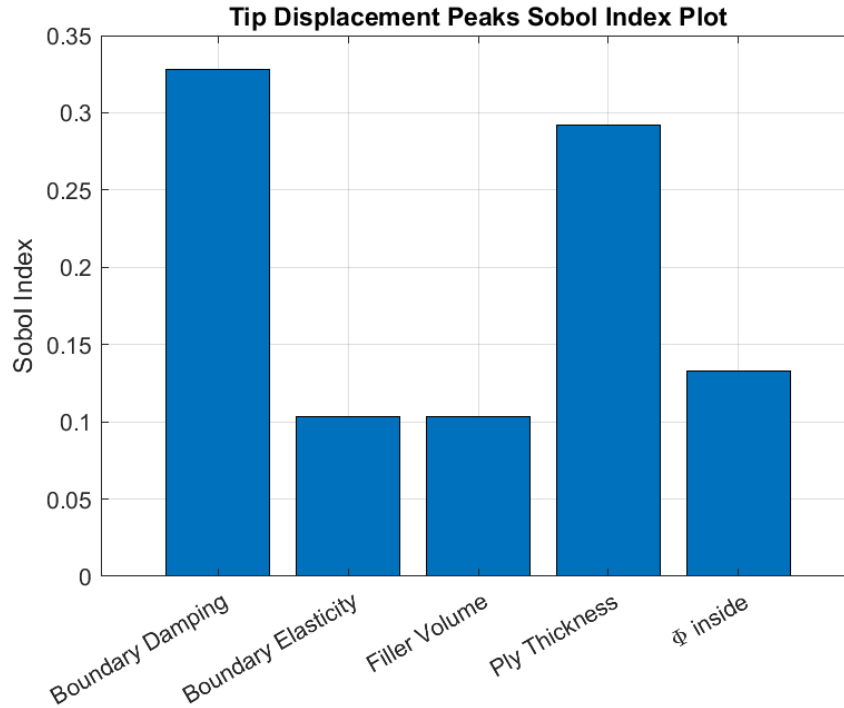
Figure 22: Boruta Influence Chart for Beam Weight (a) and Fundamental Frequency (b).

Figure 23 (a) shows the Sobol indices for rotation imparted on the system after deployment of the beam. The largest index value comes from boundary damping. Interestingly, the boundary damping 2-D correlation shows that there is an inconclusive relation between the boundary damping and stiffness on rotation imparted on the system. The high Sobol index could be due to a large percentage of the feasible designs had a similar stiffness and damping value at the boundary. Per Figure 23 (a), the beam's geometric makeup is also influential in body rotation of the system after deployment, agreeing with the conclusion from the Boruta chart for this same output.

Beam tip displacement upon deployment in Figure 23 (b) also shows high Sobol index values for boundary condition stiffness and damping. Again, here the weak relation between the damping value at the boundary and the deployment tip displacements of the beam from the 2D correlations show the Sobol plot for this variable may not be accurate. We also see high Sobol indices for beam cross-sectional parameters for beam tip displacements, agreeing with the Boruta influence charts in Figure 22 (b). Though relations between some inputs and the deployment characteristics of the beam were not clear in the 2-D correlations of the prior section, the Sobol and Influence charts plots are able to provide better understanding between input and output relationships from the optimization.



(a)



(b)

Figure 23: Sobol Index Chart for Beam Tip Displacements (a) and Avg Body Rotation (b).

Overall, the Boruta influence charts and Sobol index charts were able to provide helpful understanding between input and output correlations. These plots add to our observations of 2-D correlations in the prior section and provide additional context as to which inputs into the optimization are influential to the tracked outputs. Ultimately, the influence charts show that the beam’s lenticular cross- section is the most significant variable in determining the outcome of output variables in the optimization.

5. Producibility of Feasible Designs

The optimization was run for nearly 300 design iterations of which 105 of those designs were deemed feasible. We can further narrow down these feasible designs into the context of producibility by using the guidelines set in Section III. Of the pool of 105 designs that were

feasible, 60 of them were both producible and feasible. From this optimization, nearly 60% of the feasible designs were producible. The majority of these feasible designs had a ply thickness of 1.4E-03 inches, and all ply thicknesses in the producible pool fell into the “Thin” category from Table 4. Also interesting is that 90% of all feasible, producible designs had a taper ratio above 0.6. This indicates that the producible designs found overwhelmingly prefer a cross-section that is nearly consistent along the length of the beam. The producibility factor that is described in Section III allows for context of manufacturability that can help further deduce the feasibility of a design that is produced from the optimization.

C. Local vs Global Optimum

The question of local vs global optimum must be discussed when completing an optimization. Having completed an optimization study that clearly found feasible designs, another auxiliary study was performed with a different input design to see if the optimum found is local or global. Table 7 below shows the input for the optimization study described Section IV. B and input for the auxiliary optimization run. The aim of this additional optimization run investigate differences between the best feasible design from the main optimization study and the auxiliary study starting from a different input condition.

Table 7: Input Parameter Differences in Main and Auxiliary Optimization Studies

Parameter Name	Main Optimization Input	Auxiliary Optimization Input	% Difference
----------------	-------------------------	------------------------------	--------------

Weight (lb)	0.13	0.65	400%
Strain Energy (lbf-in)	1.03	12.17	1082%
Frequency (Hz)	0.61	0.87	43%
Fiber Tension	0.02	0.01	50%
Fiber Compression	0.02	0.01	50%
Matrix Tension	0.44	6.20	1309%
Matrix Compression	0.07	0.26	271%
Root Height (in)	4.57	5.93	30%
Body Rotation Rate (deg/s)	-	0.03	-
Tip Displacement Peaks	-	1.00	-
Ply Thickness (in)	7.50E-04	1.90E-03	153%
R ₂ Root (in)	1.33	2.33	75%
Root θ (deg)	28.53	25.00	12%
R ₁ Root (in)	1.25	2.17	74%
Taper Ratio, s	0.30	0.78	160%
Fiber Index	T300	E-Glass	-
Matrix Index	5505	5505	-

The auxiliary study was run for 75 design iterations in which the search algorithm was able to find 12 feasible designs. The correlations of this optimization results will not be presented in this section, rather the difference between the lenticular beam design from this auxiliary study will be compared to the main optimization study. Table 8 shows the tabulated parameters from both studies and the resulting percent differences. Overall, there exists subtle changes in the final best feasible design parameters and performance. The lenticular cross-section between both studies remains similar, with a small change in the matrix selection in the auxiliary study. The small differences in the overall design between the studies leads to very similar performance in beam's deployment behavior and stored strain energy when wrapped.

Table 8: Parameter Differences in Main and Auxiliary Optimization Studies for Best Feasible Design

Parameter Name	Main Optimization Best Feasible Design	Auxiliary Optimization Best Feasible Design	% Difference
----------------	--	---	--------------

Weight (lb)	0.42	0.40	5%
Strain Energy (lbf-in)	9.60	6.82	29%
Frequency (Hz)	1.00	0.73	27%
Fiber Tension	0.02	0.02	0%
Fiber Compression	0.05	0.09	80%
Matrix Tension	0.15	0.17	13%
Matrix Compression	0.03	0.00	100%
Root Height (in)	6.28	6.80	8%
Body Rotation Rate (deg/s)	0.02	0.03	50%
Tip Displacement Peaks	1.00	1.00	0%
Ply Thickness (in)	7.50E-04	1.00E-03	33%
R ₂ Root (in)	3.00	3.00	-
Root θ (deg)	25.00	32.00	28%
R ₁ Root (in)	1.90	1.30	32%
Taper Ratio, s	0.78	0.70	10%
Fiber Index	T300	T300	-
Matrix Index	5505	319	-

Due to the similar design and performance seen in the design from the auxiliary study, it cannot be clearly deduced whether the best feasible design obtained in the main optimization was a local or global optimum. Instead, it can be noted that the auxiliary study had converged to the same local optimum from the main study. Perhaps the selection of the input parameters in the auxiliary study was too closely related to a feasible design from the main optimization and thus caused this convergence in beam design. It may be beneficial to run a future optimization with an input design with a much larger difference in beam parameters to determine if more local optima exist and then determine if a global optimum has been found.

V. Conclusion & Future Work

In this paper, an algorithm is presented to evaluate deployable composite beam structures to meet both mission requirements and structural survival of the beam upon deployment. The algorithm includes a modal analysis to analyze the fundamental mode of the deployed system and a series of

nonlinear FEA simulations to simulate performance of the beam as it is wrapped and deployed. Addition of the deployment simulation within the optimization loop allows for the algorithm to analyze performance of a beam design as it is deployed and can adjust design parameters based on this performance. The optimization has the ability to manipulate the composite material properties and cross-section shape of the lenticular opening of the beam to find the most feasible design. This paper also introduces a new beam design parameter to taper the beam and analyze the effects of a chordwise taper on wrapping and deployment characteristic. The paper introduces a method to determine producibility of feasible designs for manufacture based on a ply thickness and associated Poisson's ratio. Lastly, further exploration of the design space is discussed with discussion of local and global optimums.

Using the SHERPA algorithm, nearly 100 designs were evaluated, of which 37% were deemed feasible based on the objective function and constraints. The best feasible design from the optimization consisted of a light beam with a small lenticular opening and relatively consistent cross-section along the length of the beam. The resulting deployment characteristics were also unaggressive with small rotation imparted on the system and minimal oscillations measured at the beam's tip. Correlations between the objective variables are examined, showing strong positive correlation between stored strain energy and weight of a beam design. Small amounts of clustering were seen in the lower range of the beam weight, strain energy and beam displacements, indicating that designs were adhering to the minimization of the objective variables. Although clustering was seen, the data at those regions also showed some spread pointing to the unpredictability of the beam's deployment.

Parameter correlations using 2D plots were observed for the optimization's various input variables. The taper ratio showed strong correlation to beam weight, but perhaps most importantly, showed

that designs from the optimization tended to prefer a less aggressive taper ratio i.e., a more constant cross-section design. Ply thickness showed strong positive correlations in relation to beam weight, strain energy and deployed frequency, validating concepts understood from classical structural mechanics. Root θ correlations showed that the optimization preferred designs with smaller lenticular openings. Sobol and Boruta influence charts were also analyzed to add to our observations of 2-D correlations and provide additional context as to which inputs into the optimization are influential.

Discussion regarding global or local optimums were also discussed from the optimizations results. An auxiliary optimization was conducted at a different input condition to see if the results of that auxiliary study would converge to similar beam design obtained from the main optimization. This additional study produced a similar best design to the main optimization which could be contributed to too similar of a starting input design to that of the main study. Thus, it could be concluded that a local optimum was found, but whether the design was a global optimum remained inconclusive.

Perhaps one of the largest hindrances in this optimization algorithm is the long solution time for each design iteration evaluation. Inclusion of the nonlinear dynamic analysis in the optimization slows down the optimization algorithm's ability to search for feasible designs. Future work can utilize HEEDS' ability to deploy high power computing (HPC) clusters to run the simulation and allow SHERPA to analyze more designs in less time. Given enough data produced, a response surface can be produced to better understand the relationship between the various input and output parameters without the need for explicit computation. HEEDS' latest design space exploration algorithm, SHERPA AI, could also be utilized to find a feasible design in less iterations. Additionally, future work can expand the material property database used in this paper and include

the composite micromechanics calculation in the optimization loop. The ability to find the strength capability of a particular combination of fiber, matrix and filler volume combination will allow for of a larger array of material combinations to be assessed. Ultimately the algorithm presenting in this paper aims to automate the virtual prototyping process in optimizing flexible composite deployable structures and reduce standard industry process time by several orders of magnitude.

VI. Bibliography

- [1] White, A. (2016) Northrop Grumman's Astro Aerospace Completes NISAR Reflector Preliminary Design Review Available at: <https://investor.northropgrumman.com/news-releases/news-release-details/northrop-grummans-astro-aerospace-completes-nisar-reflector> (Accessed: 2024).
- [2] R. Tulloss, " Optimization of Geometric Parameters for a Deployable Space Structure", MS Thesis Virginia Polytechnic Institute and State University, Blacksburg, VA 2021.
- [3] Z. Fink, " Optimization of Geometric Parameters and Material Properties for a Flexible Deployable Space Structure," MS Thesis Virginia Polytechnic Institute and State University, Blacksburg, VA, 2022.
- [4] M. Sibai, "Optimization of an Unfurlable Space Structure," M.S. Thesis, Kevin T. Crofton Department of Aerospace and Ocean Engineering, Virginia Polytechnic Institute and State University, Blacksburg, VA, 2020.
- [5] Airbus Defense and Space SAS, HCA 4-1 Hight Capacity Actuator for Small Satellites (2023), Available at: <https://www.airbus.com/en/products-services/space/equipment/avionics/agile-actuators>
- [6] Freeland, R. E., Garcia, N. F., Iwamoto, H. "Wrap-Rib Antenna Technology Development," Large Space Antenna Systems Technology, 1984, pp. 139-166.
- [7] W. Wang, H. Rodrigue and a. S.-H. Ahn, "Deployable Soft Composite Structures," Sci Rep, vol. 6, 2016.
- [8] Francis, W H et al., "High Strain Composite Slit Tubes for Roll-Out Structures," in AIAA Spacecraft Structures Conference, Kissimmee, FL, 2015.

- [9] J. Winter et al., "A proposed large deployable space structures experiment for high power, large aperture missions in MEO," in IEEE Aerospace Conference Proceedings (IEEE Cat. No.04TH8720), pp. 532 Vol.1, doi: 10.1109/AERO.2004.1367636, 2004.
- [10] B. Gaudi, S. Seager, B. Mennesson and A. Kiessling, "Habex: The habitable exoplanet observatory interim report," NASA Astronomy, Physics and Space Technology Directorate, Pasadena, CA, 2018.
- [11] M. Mobrem and D. Adams, "Deployment analysis of the lenticular jointed antennas onboard the Mars Express spacecraft," Journal of Spacecraft and Rockets, vol. 46, no. 2, pp. 394-402, 2009.
- [12] S. Surma, "Composite Materials: Mechanics, Manufacturing and Modeling," First Edition, CRC Press, 2021
- [13] Z. Hashin, "Failure Criteria for Unidirectional Fiber Composites," Journal of Applied Mechanics, vol. 47, pp. 329-334, 1980.
- [14] ABAQUS, Structural Analysis, Software Package, Ver. 2019, Dassault Systèmes, Vélizy-Villacoublay, France.
- [15] T. Neigh, "Local and Global Sensitivity Analysis of Thin Ply Laminated Carbon Composites," MS Thesis Virginia Polytechnic Institute and State University, Blacksburg, VA, 2024.
- [16] D. H. Kwak, H. Y. Jung, J. E. Lee and K. H. Knag, "Material Analysis and Shape Optimization of a Deployable Lightweight Satellite Antenna Reflector," Journal of the Korean Society of Manufacturing Technology Engineers, vol. 26, no. 2, pp. 185-192, 2017.

- [17] P. Fernandes, R. Marques, R. Pinto, P. Mimoso, J. Rodrigues, A. Silva, J. Tavares, G. Rodrigues and N. Correia, “Design and Optimization of A Self-Deployable Composite Structure” *Materiales Compuestos*, vol. 04, no. 1, pp. 80-89, 2022
- [18] HEEDS, Optimization Formulation, Software Package, Ver. 2020.1, Siemens, Munich, Germany.
- [19] Helius, Autodesk, Ver. 2017. [Online]. Available:
<https://knowledge.autodesk.com/support/helius-composite/learn-explore/caas/CloudHelp/cloudhelp/2017/ENU/ACMPDS/files/GUID-2B4538D7-227F-4C9F-891F-785F90CA10CA-htm.html>
- [20] HEEDS, “Guidelines toward the number of evaluations in a parameter optimization study using SHERPA”, Siemens, Munich, Germany, 2018.
- [21] Kursa, M. B., “Boruta for those in a hurry,” *The Comprehensive R Archive Network*
Available: <https://cran.r-project.org/web/packages/Boruta/vignettes/inahurry.pdf>.
- [22] Zhang, X., Trame, M., Lesko, L., and Schmidt, S., “Sobol Sensitivity Analysis: A tool to guide the development and evaluation of Systems Pharmacology Models,” *CPT: Pharmacometrics & Systems Pharmacology*, vol. 4, Feb. 2015, pp. 69–79.

Appendix A: Hashin Damage Initiation Criteria

The survival of the structure throughout the wrapping process is ensured by looking at the Hashin composite damage initiation criteria within ABAQUS. The composite failure modes are fiber tension, fiber compression, matrix tension, and matrix compression, and the failure criterion calculation for each are shown in Eq. 5-8 [12].

$$\text{Fiber Tension} = \left(\frac{\hat{\sigma}_{11}}{X^T}\right)^2 + \alpha \left(\frac{\hat{\tau}_{12}}{S^L}\right)^2 \quad (5)$$

$$\text{Fiber Compression} = \left(\frac{\hat{\sigma}_{11}}{X^T}\right)^2 \quad (6)$$

$$\text{Matrix Tension} = \left(\frac{\hat{\sigma}_{22}}{Y^T}\right)^2 + \left(\frac{\hat{\tau}_{12}}{S^L}\right)^2 \quad (7)$$

$$\text{Matrix Compression} = \left(\frac{\hat{\sigma}_{22}}{2S^T}\right)^2 + \left[\left(\frac{Y^C}{2S^T}\right)^2 - 1 \right] \frac{\hat{\sigma}_{22}}{Y^C} + \left(\frac{\hat{\tau}_{12}}{S^L}\right)^2 \quad (8)$$

X^T = Longitudinal tensile strength

X^C = Longitudinal compressive strength

Y^T = Transverse tensile strength

Y^C = Transverse compressive strength

S^L = Longitudinal shear strength

S^T = Transverse shear strength

α = Coefficient for the fiber tension shear stress contribution

$\hat{\sigma}$ = Stress Tensor

Appendix B: HEEDS Material Property Selection Repository

Table B1: HEEDS Material Property Selection Repository [17]

Fiber	Matrix	Filler Volume	S1 (Tensile longitudinal)	neg S1 (Compression longitudinal)	S2 (Tensile translation)	neg S2 (compression translation)	S12 (longitudinal shear)	S2 (pos)	S32 (longitudinal shear)
Eglass	319	0.45	1.40E+05	9.46E+04	7.94E+03	1.47E+04	1.81E+04	1.47E+04	5625.354545
Eglass	319	0.5	1.56E+05	1.05E+05	8.08E+03	1.50E+04	1.84E+04	1.50E+04	5722.704517
Eglass	319	0.55	1.72E+05	1.16E+05	8.23E+03	1.53E+04	1.88E+04	1.53E+04	5832.622284
Eglass	319	0.6	1.87E+05	1.26E+05	8.40E+03	1.56E+04	1.91E+04	1.56E+04	5953.468811
Eglass	319	0.65	2.03E+05	1.37E+05	8.59E+03	1.59E+04	1.96E+04	1.59E+04	6083.86439
Eglass	5505	0.45	1.40E+05	9.46E+04	8.24E+03	2.46E+04	9.64E+03	2.46E+04	7614.40705
Eglass	5505	0.5	1.56E+05	1.05E+05	8.37E+03	2.50E+04	9.79E+03	2.50E+04	7731.696711
Eglass	5505	0.55	1.72E+05	1.16E+05	8.51E+03	2.54E+04	9.96E+03	2.54E+04	7864.152733
Eglass	5505	0.6	1.87E+05	1.26E+05	8.67E+03	2.59E+04	1.01E+04	2.59E+04	8009.750684
Eglass	5505	0.65	2.03E+05	1.37E+05	8.84E+03	2.64E+04	1.03E+04	2.64E+04	8166.874806
T300	319	0.45	2.30E+05	1.42E+05	8.05E+03	1.50E+04	1.81E+04	1.50E+04	5705.091421
T300	319	0.5	2.56E+05	1.58E+05	8.18E+03	1.52E+04	1.85E+04	1.52E+04	5797.488312
T300	319	0.55	2.82E+05	1.74E+05	8.33E+03	1.55E+04	1.88E+04	1.55E+04	5901.845882
T300	319	0.6	3.07E+05	1.90E+05	8.49E+03	1.58E+04	1.92E+04	1.58E+04	6016.525748
T300	319	0.65	3.33E+05	2.06E+05	8.67E+03	1.61E+04	1.96E+04	1.61E+04	6140.286371
T300	5505	0.45	2.30E+05	1.42E+05	9.11E+03	2.72E+04	9.88E+03	2.72E+04	8417.407132
T300	5505	0.5	2.56E+05	1.58E+05	9.18E+03	2.75E+04	1.00E+04	2.75E+04	8484.834585
T300	5505	0.55	2.82E+05	1.74E+05	9.26E+03	2.77E+04	1.02E+04	2.77E+04	8560.96415
T300	5505	0.6	3.07E+05	1.90E+05	9.35E+03	2.80E+04	1.03E+04	2.80E+04	8644.655964
T300	5505	0.65	3.33E+05	2.06E+05	9.45E+03	2.83E+04	1.05E+04	2.83E+04	8734.967097

Appendix C: Preliminary Optimization Figures

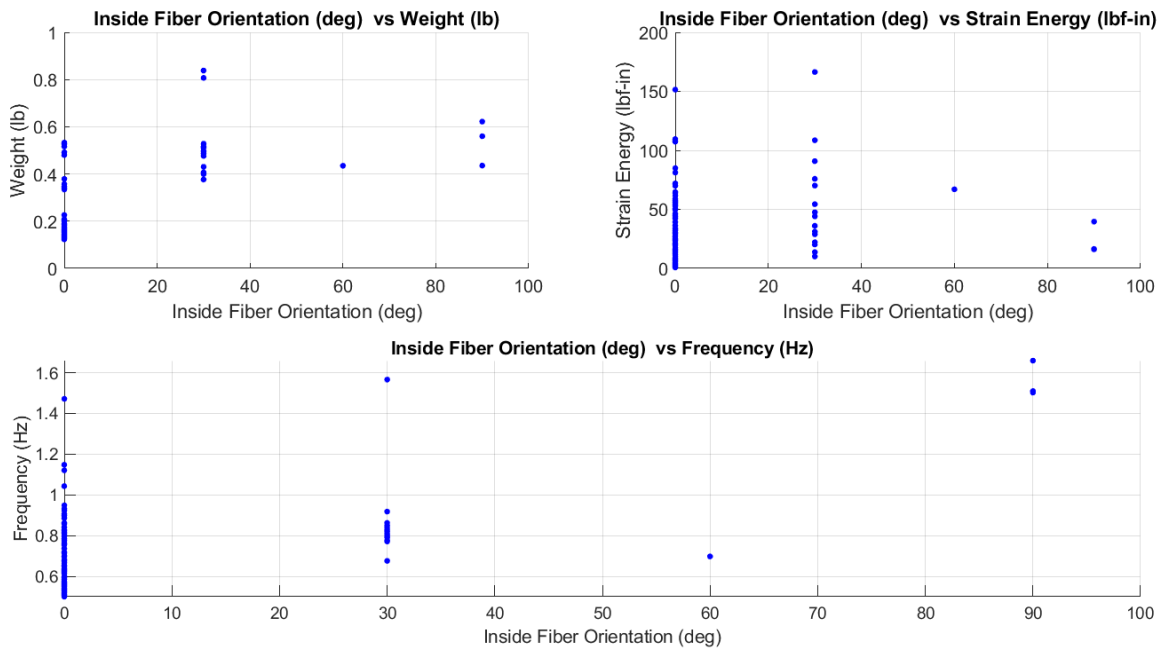


Figure 24: Parameter Correlation: Inside Fiber Orientation vs Weight (a), Strain Energy (b) & Frequency (c)

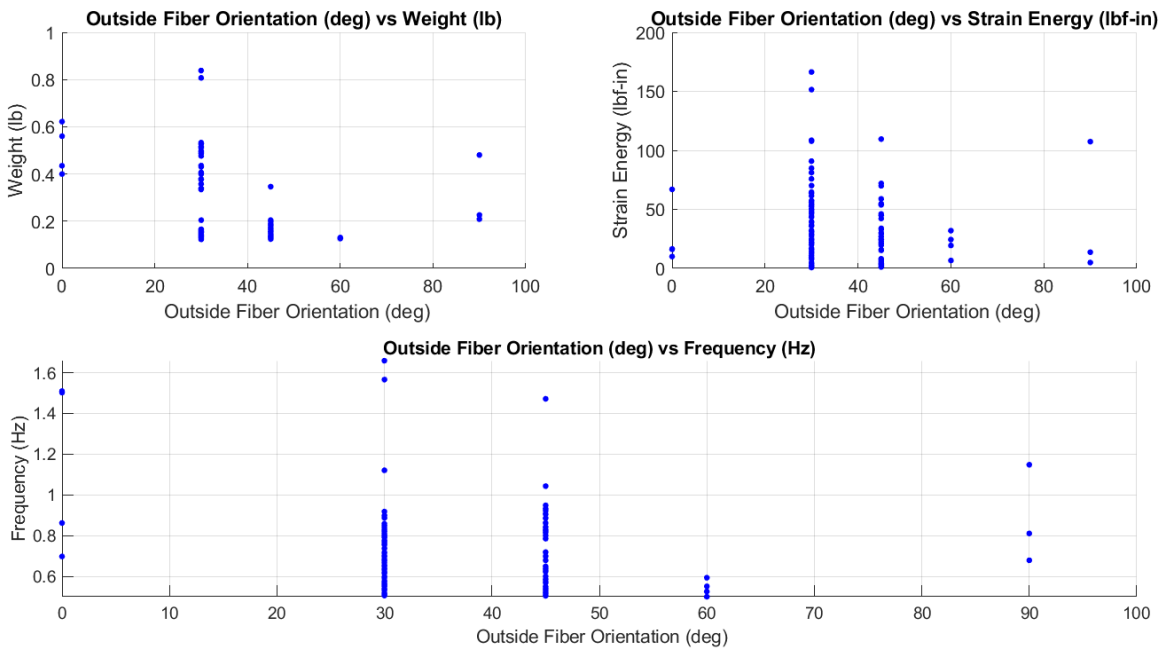


Figure 25: Parameter Correlation: Inside Fiber Orientation vs Weight (a), Strain Energy (b) & Frequency (c)

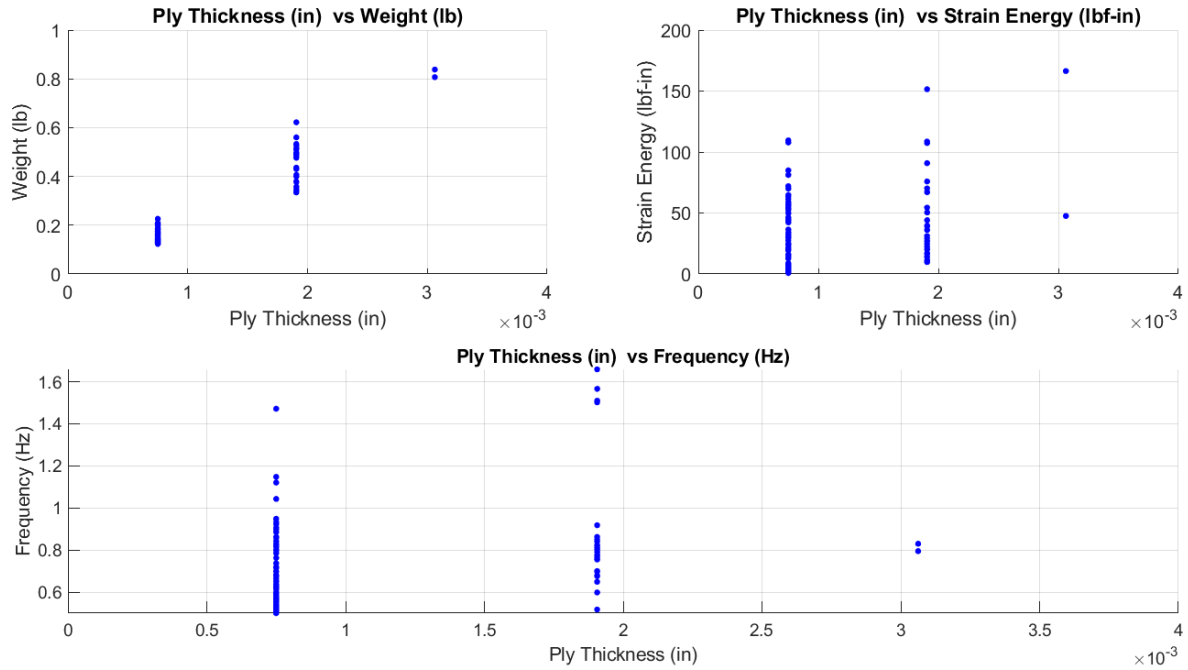


Figure 26: Parameter Correlation: Ply Thickness vs Weight (a), Strain Energy (b) & Frequency (c)

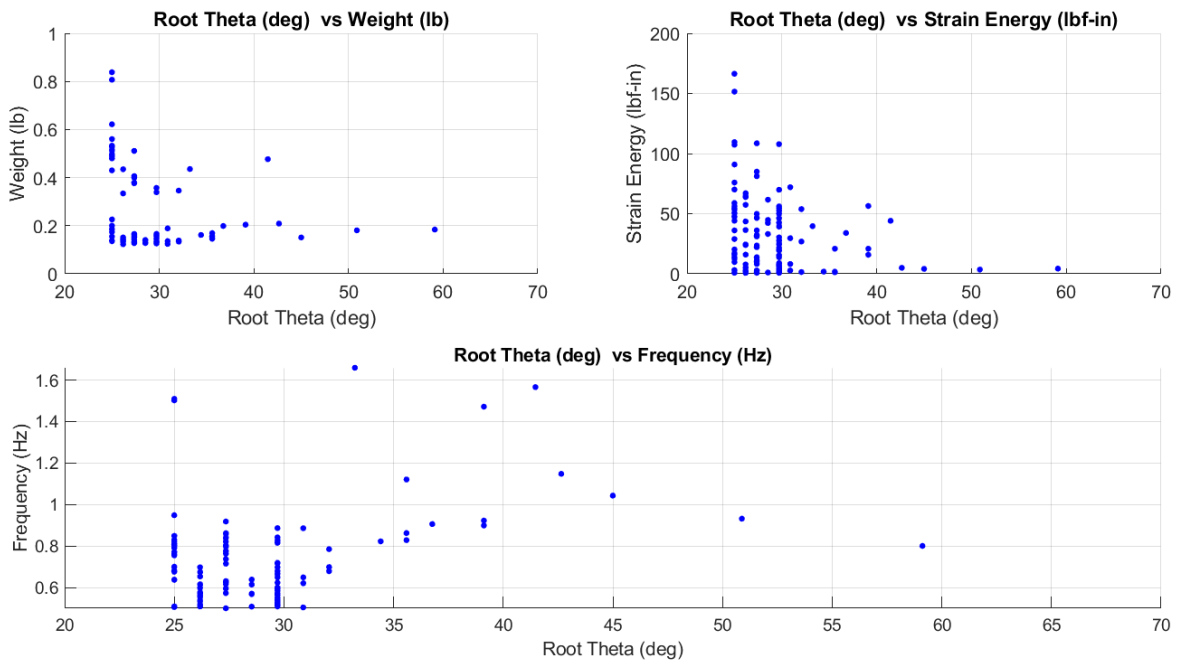


Figure 27: Parameter Correlation: Root θ vs Weight (a), Strain Energy (b) & Frequency (c)

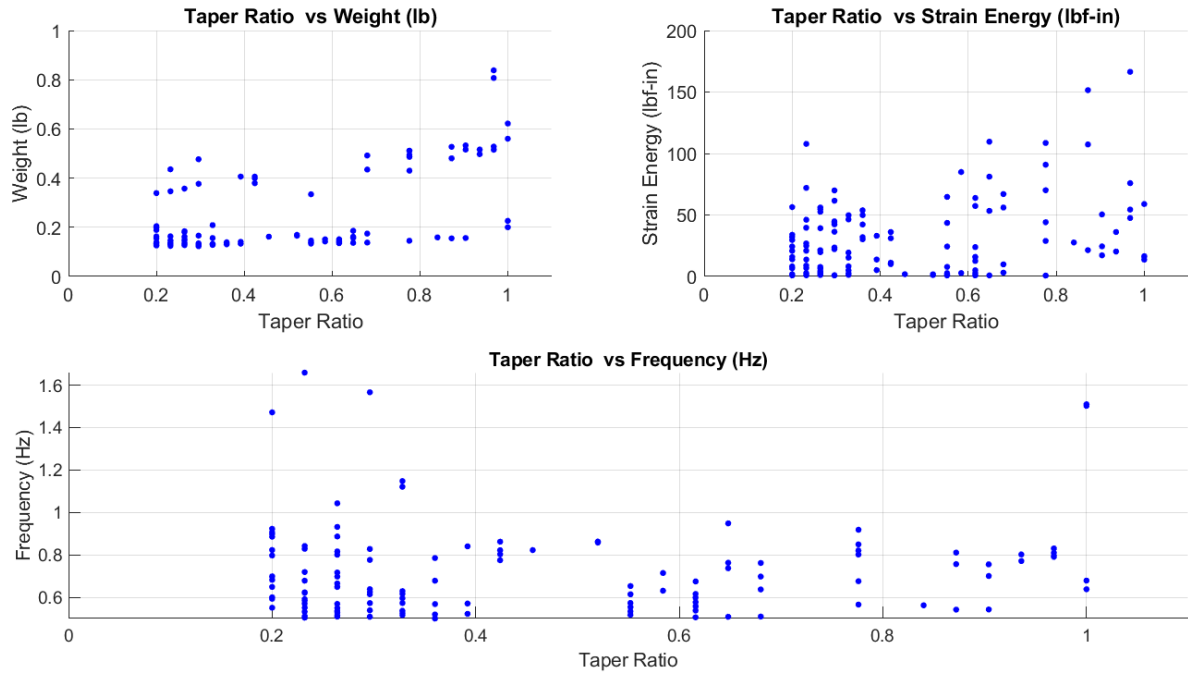


Figure 28: Parameter Correlation: Taper Ratio vs Weight (a), Strain Energy (b) & Frequency (c)

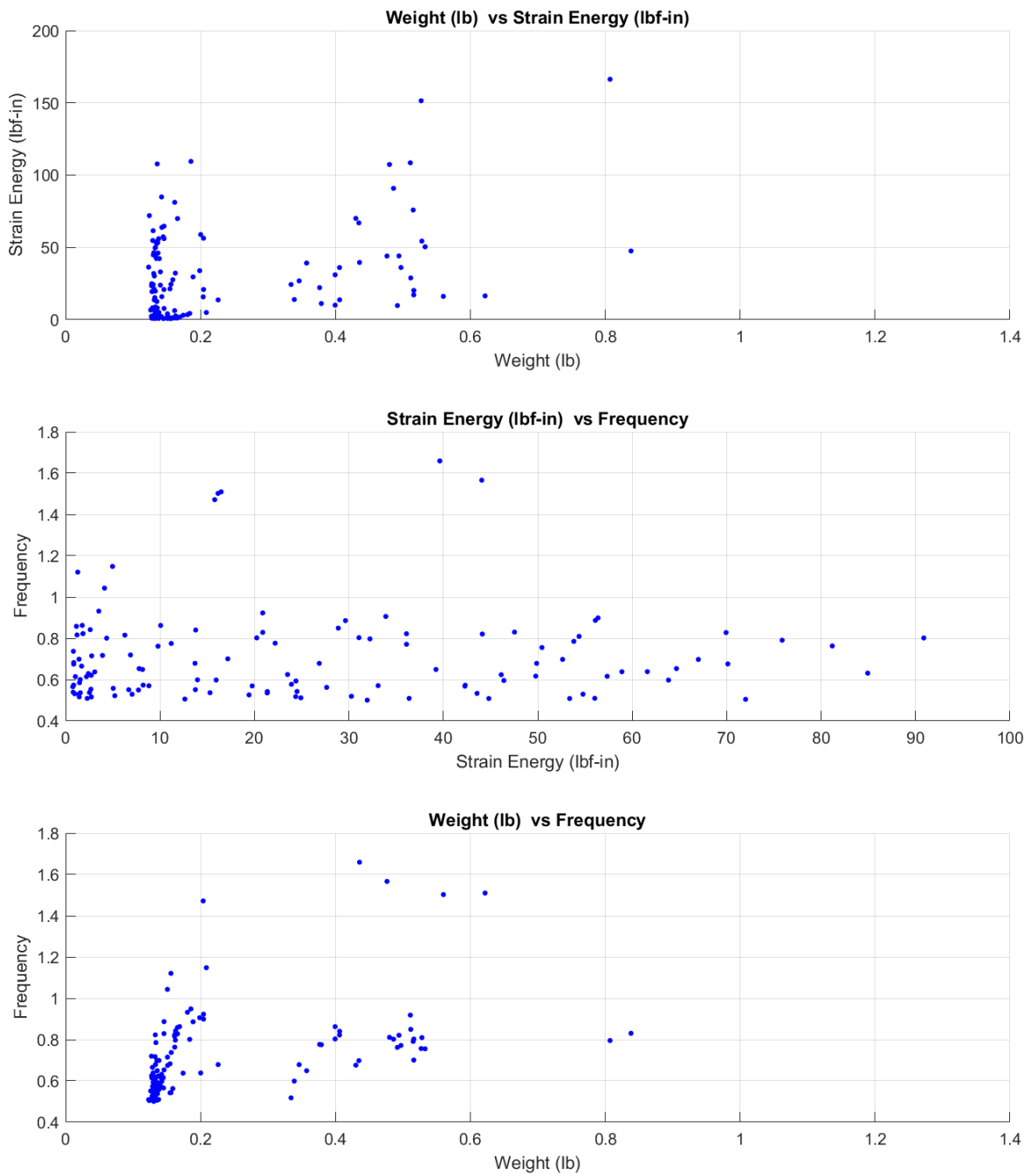


Figure 29: Objective Correlation: Strain Energy vs Weight (a), Frequency vs Strain Energy (b) & Weight vs Frequency (c)

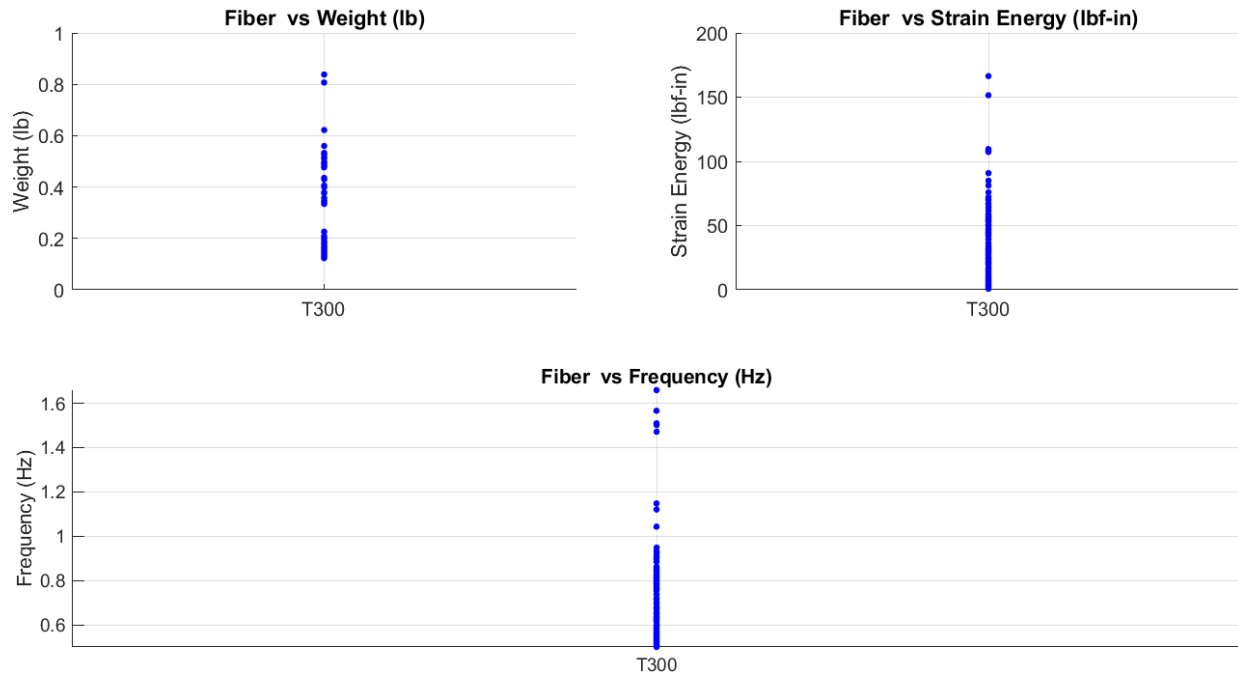


Figure 30: Parameter Correlation: Fiber Selection vs Weight (a), Strain Energy (b) & Frequency (c)

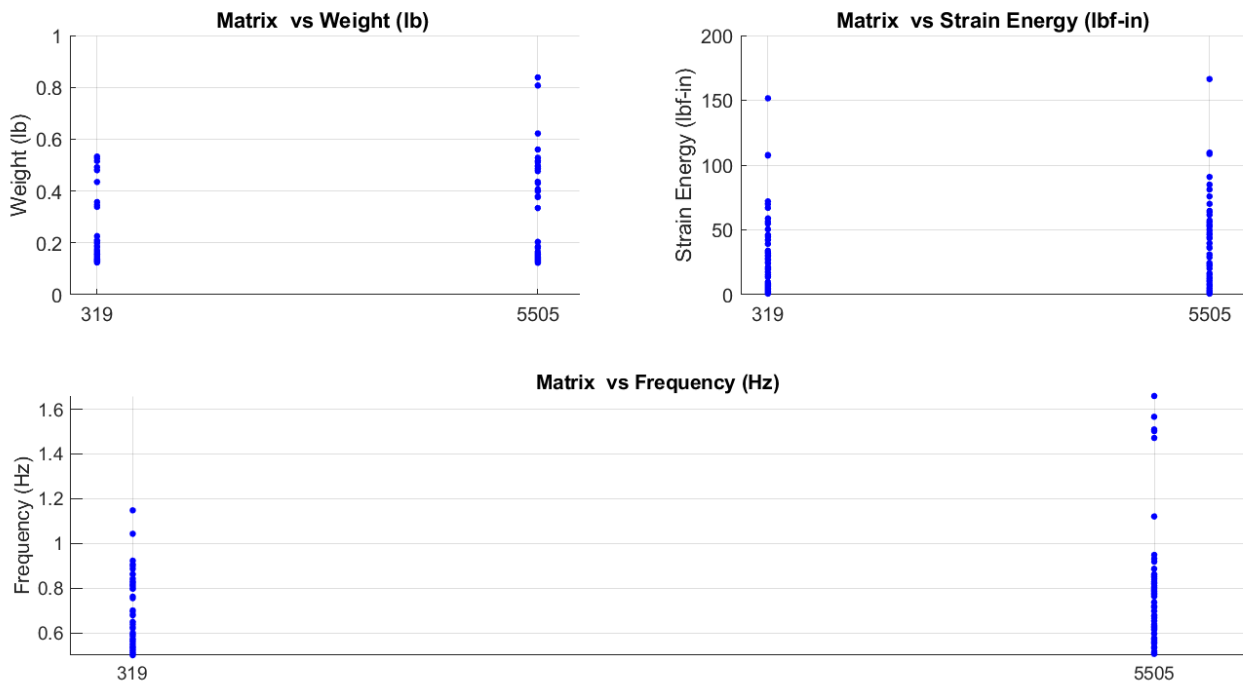
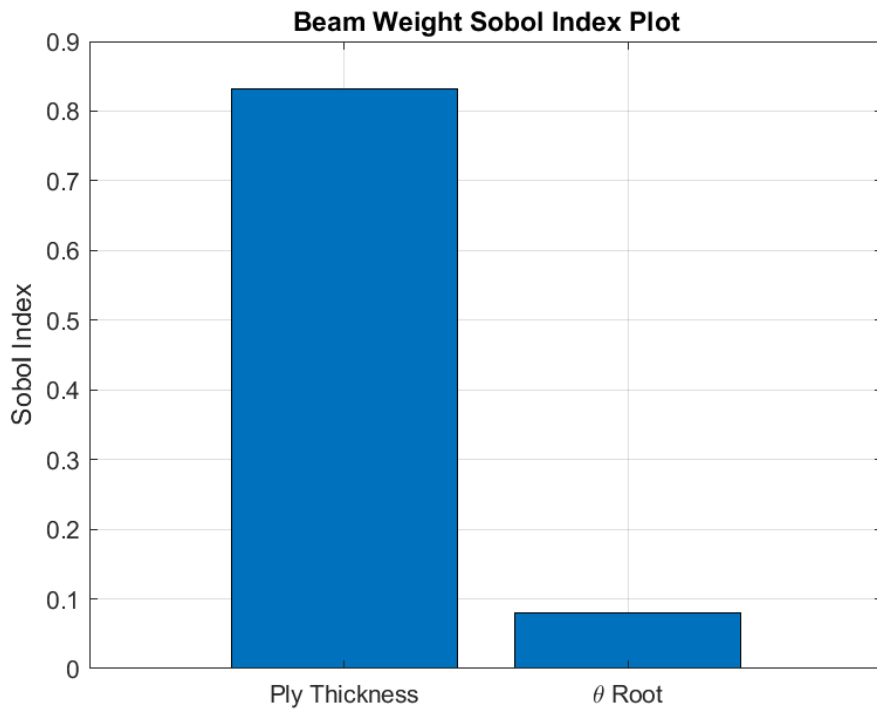
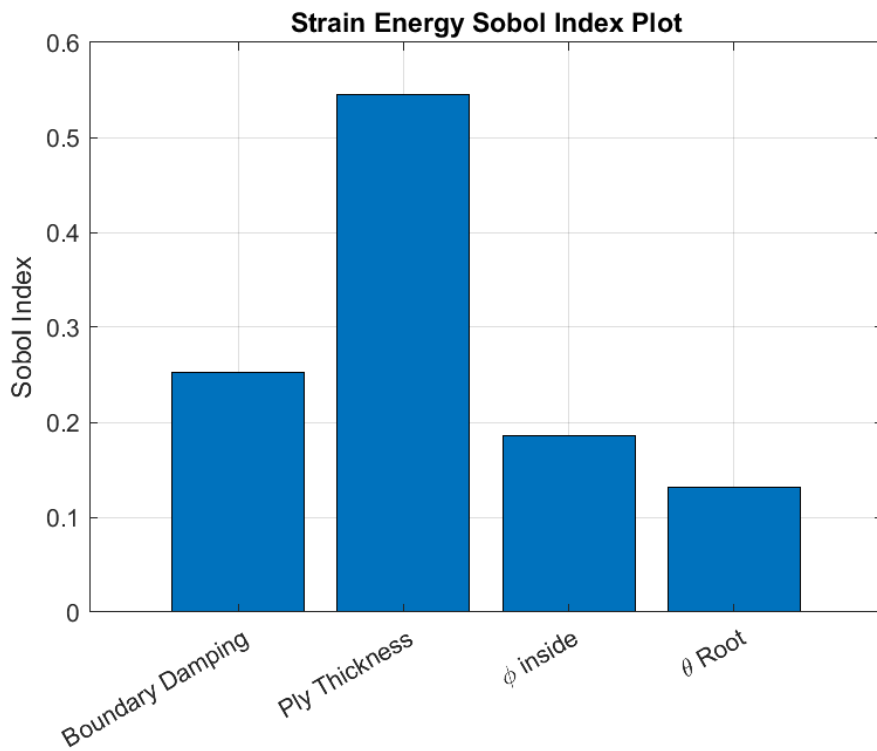


Figure 31: Parameter Correlation: Matrix Selection vs Weight (a), Strain Energy (b) & Frequency (c)

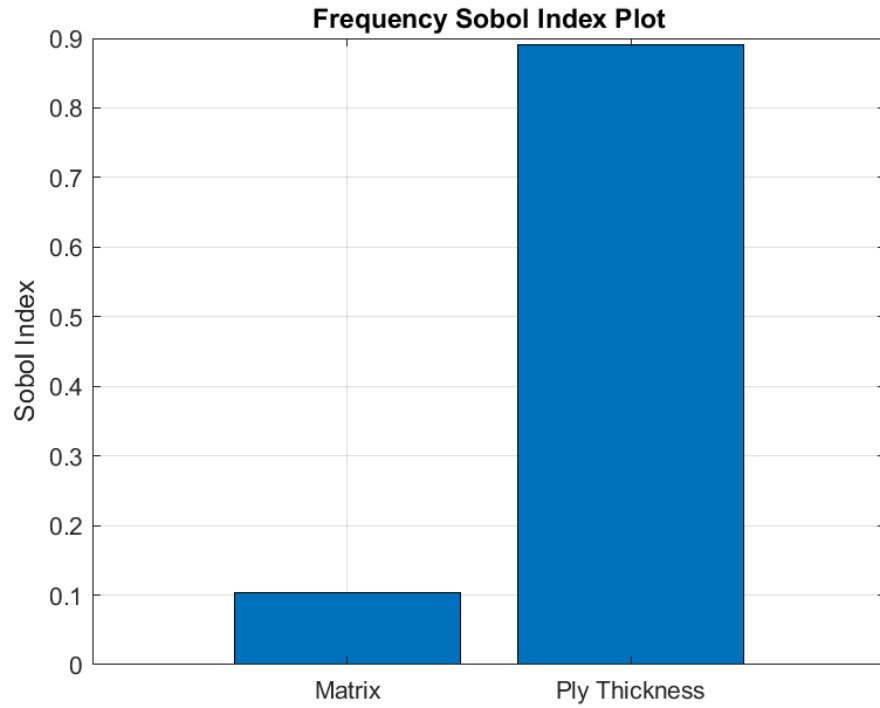
Appendix D: Additional Sobol Index Plots



(a)



(b)



(c)

Figure 32: Sobol Index Plot Correlation: Beam Weight (a), Strain Energy (b) & Deployed Frequency (c)